www.ucm.es/info/estratig/journal.htm

Journal of Iberian Geology 39 (2) 2013: 203-222
http://dx.doi.org/10.5209/rev_JIGE.2013.v39.n1.41759

Journal of Iberian Geology
AN INTERNATIONAL PUBLICATION OF EARTH SCIENCES

The Upper Triassic alkaline magmatism in the NW Iberian Chain (Spain)

El magmatismo alcalino del Triásico Superior en el NO de la Cadena Ibérica (España)

T. Sanz, M. Lago, A. Gil, C. Galé*, J. Ramajo, T. Ubide, A. Pocoví, P. Tierz, P. Larrea

Earth Sciences Department, University of Zaragoza, C/ Pedro Cerbuna 12, 50009 Zaragoza, Spain

**corresponding autor: carlos.gale@gmail.com*

Received: 29/08/2012 / Accepted: 08/12/2012

Abstract

We have carried out a complete study of the Upper-Triassic alkaline magmatism on the northwestern margin of the Iberian Chain. This magmatism is composed of mafic sills, which intrude the Keuper facies in two geographic sectors: the Cameros Massif (NW) and the Moncayo Massif (SE). In both of these sectors, the rocks are characterised by an intense alteration (spilitisation).

The field relationships point to an Upper Triassic age for the studied sills, given that: 1) interactions are recognised between the magma and wet, unconsolidated host sediments, suggesting that the magma was emplaced during or shortly after the deposition of the Keuper facies; 2) in the Moncayo sector a conglomerate bed that includes igneous clasts overlaies the sills and passes upwards to the Norian-Rhaetian Imón Fm.

According to the petrological and geochemical features of the sills, an internal differentiation can be recognised inwards, with the developments of three zones: chilled margins, central facies and pegmatoid facies. The rocks are porphyritic and are mainly composed of phenocrysts of pseudomorphed olivine and microcrysts of plagioclase, opaque minerals and minor clinopyroxene. Vesicles and xenoliths of the host sedimentary rocks are also recognised, especially at the chilled margins. The mineral assemblage is constant across the sills but the mineral proportions vary among the different zones.

The sills are basic to intermediate rocks. They are classified as basalts to dacites with an alkaline geochemical affinity. According to the trace element contents, this magmatism is related to an enriched sub-lithospheric mantle source affected by crustal contamination.

Considering the Upper Triassic magmatisms from southwestern Europe, two types can be distinguished. On the one hand, the magmatisms in the Catalonian Coastal Ranges and SE France are paleogeographically located in the inner platform and are related to deep, astenospheric mantle sources with no evidence of crustal contamination. On the other hand, the magmatisms in the NW Iberian Chain –this study-, the External Betics and the Brescian Prealps are situated in a more litoral position and are related to a shallower, lithospheric mantle with evidence of crustal contamination. These differences could be related to the thickness of the continental crust, which might be thinner in the inner areas of the platform.

Keywords: sill, spilitisation, alkaline, Upper Triassic, Iberian Chain

Resumen

Se ha realizado un estudio completo del magmatismo alcalino del Triásico Superior del margen noroccidental de la Cadena Ibérica. Este magmatismo consta de sills máficos emplazados entre los materiales sedimentarios de la Facies Keuper en dos sectores:

Macizo de Cameros (NO) y Macizo del Moncayo (SE). En ambos sectores, las rocas estudiadas se caracterizan por una intensa alteración (espilitización).

Las relaciones de campo apuntan a una edad de los sills estudiados de Triásico Superior dado que: 1) se reconocen interacciones entre el magma y el sedimento encajante sin consolidar, que sugieren su emplazamiento coetáneo con el depósito de la facies Keuper o poco posterior y, 2) se observa, en el sector de Moncayo, un nivel conglomerático con cantos de rocas ígneas similares a las que forman los sills, depositado entre los sedimentos argilíticos que se disponen por encima de los sills y siempre, bajo la Fm. Imón de edad Noriense terminal a Retiense inferior.

Las características petrológicas y geoquímicas de los sills sugieren una diferenciación hacia el interior de los mismos, reconociéndose tres zonas: borde enfriado, facies central y facies pegmatoide. Las rocas son porfídicas y tienen una asociación mineral común formada por fenocristales de olivino alterado y una mesostasia compuesta por microcristales de plagioclasa, opacos y clinopiroxeno. También se reconocen vesículas y enclaves de la roca sedimentaria encajante, especialmente en el borde enfriado. Las proporciones modales varían entre las tres facies reconocidas.

Los sills están formados por rocas básicas a intermedias, clasificadas desde basaltos a dacitas, con afinidad alcalina. De acuerdo a sus contenidos en elementos traza, este magmatismo está relacionado con una fuente mantélica sublitosférica enriquecida, afectada por contaminación cortical.

Considerando los magmatismos del Triásico Superior del suroeste de Europa, pueden establecerse dos tipos. Por un lado, los magmatismos aflorantes en las Cadenas Costero Catalanas y el Sur de Francia estaban paleogeográficamente situadas hacia zonas internas de la plataforma y se relacionan con un manto profundo, astenosférico, sin evidencias de contaminación cortical. Por el contrario, los magmatismos de las áreas más occidentales y septentrionales (NO de la Cadena Ibérica –este estudio-, Zonas Externas de las Béticas y Prealpes de Brescia), próximas al litoral paleogeográfico, se relacionan con un manto más superficial, litosférico y muestran evidencias de contaminación cortical. Todas estas diferencias observadas pueden relacionarse con variaciones del espesor de la corteza continental, más adelgazada hacia las zonas internas de la plataforma.

Palabras clave: sill, espilitización, alcalino, Triásico superior, Cadena Ibérica

1. Introduction

The Triassic – Jurassic transition in the NE margin of the Iberian peninsula (Spain) was characterised by a strong extensional regime (Sopeña *et al.*, 1988) related to the Iberian Rift (Alvaro *et al.*, 1979). The extension was developed along listric normal faults, in the brittle – ductile transition zone of the continental crust (Gibbs, 1984; Wernicke and Tilke, 1989; Morley, 1999). The possible propagation in depth in a ramp–and–flat staircase fault model across the lithosphere and even the upper mantle is a possibility not to be discarded in the Iberian Plate (Vargas *et al.*, 2009).

Álvaro *et al.* (1979) defined the Iberian rifting as a result of a triple junction, located over a mantle plume centred in a position close to the present-day Castellón city. Salas and Casas (1993) identified four successive evolutionary stages in the basins of the eastern Iberian margin during the Mesozoic extension. The Triassic rift (Late Permian – Hettangian) is the first of these stages; it comprised a tectonic subsidence phase followed by a long period of thermal subsidence (López Gómez *et al.*, 1993; Arche and López Gómez, 1996).

An Upper Triassic alkaline magmatic province was developed at the end of the Triassic rift stage (Lago *et al.*, 1996). This magmatic province is characterised by similar geochemical, petrological and emplacement conditions. It comprises outcrops in the NW part of the Iberian Chain (Aragonian Branch), in the Catalonian Coastal Ranges (Tarragona and Mallorca) and southern France (Corbières, Écrins-Pelvoux and Provence). It is associated to the intracontinental rifting of the western margin of the Neotethys, over an asthenospheric mantle source (Lago *et al.*, 1996; Bastida *et al.*, 1989).

The Upper Triassic alkaline magmatism in the northwestern Iberian Chain consists of a hypovolcanic complex emplaced into the Keuper facies in two geographic sectors (Fig. 1): a) the N front of the Cameros Massif (La Rioja), and b) the Moncayo Massif (Soria and Zaragoza). This complex has been partially studied by Bastida *et al*. (1989) and Sanz *et al*. (2012a). A complete study of this magmatism, however, has not been carried out up to date.

Recently, Pérez-López *et al*. (2012) have described a Norian subalkaline magmatism related to the Triassic rift in the external part of the Betic Cordillera. This magmatism emplaced into the Zamoranos Fm (Pérez-López *et al*., 1992), which is correlated to the Imón Fm (Iberian Chain) and the Isábena Fm (Pyrenees) and to other carbonate units of the western Tethys realm (Pérez-López *et al*., 1992; López-Gómez *et al*., 1998; Arnal *et al*., 2002; Pérez-López and Pérez-Valera, 2007). Outside of Iberia, Upper Triassic igneous rocks also have been recognised in SE France (e.g. Corbières, Écrins-Pelvoux and Provence; Azambre and Rossy, 1981, Durand *et al*., 2011 and references therein, Vatin-Pérignon *et al*., 1974) and the Brescian Prealps (Cassinis *et al*., 2008).

The aim of this paper is to characterise for the first time the Upper Triassic magmatism in the Cameros and

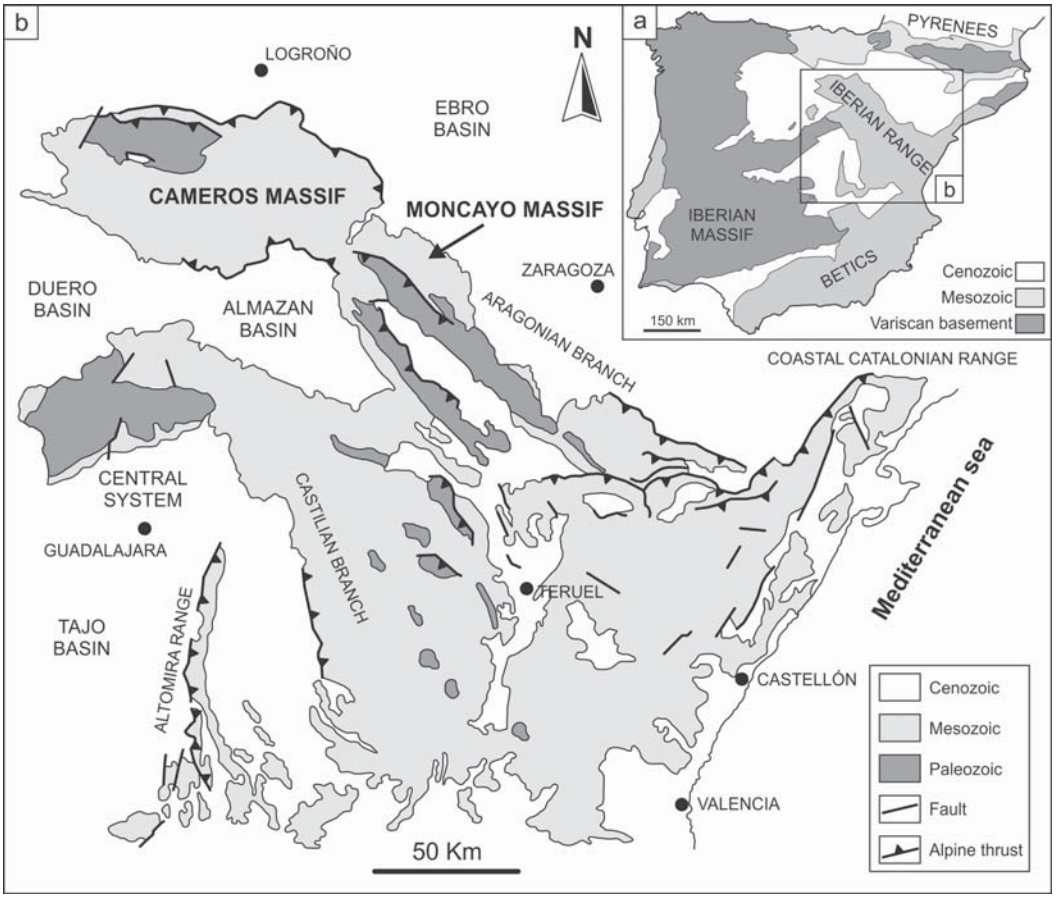

Fig. 1.- a- Main geological units of the Iberian Peninsula. b- Present-day configuration of the Iberian Ranges and location of the Cameros and Moncayo Massifs.

Fig. 1.- a- Principales unidades geológicas de la Península Ibérica. b- Configuración actual de la Cordillera Ibérica y localización de los Macizos de Cameros y Moncayo.

Moncayo sectors in order to define its emplacement age and petrogenetic features. Further, the comparison with Upper Triassic magmatisms of SW Europe allows us to establish the geodynamic implications for the western margin of the Neotethys rift.

2. Stratigraphical background

The Keuper facies in the NW part of the Iberian Chain (Aragonian Branch) is mainly composed of mudstones with interbedded evaporite levels and sporadic sandstone and dolomite levels (López Gómez *et al*., 2002). The general interpretation of the Keuper facies is that it represents sabkha deposits with more continental influence towards the west. The age of these deposits is Carnian to Norian according to pollen and spore associations (López-Gómez *et al*., 2002 and references therein). The Keuper facies is usually overlaid by the Imón Fm (Goy and Yébenes, 1977), which comprises well-stratified dolomites showing a gradual transition from the Keuper facies, representing carbonate-evaporite tidal flat deposits of latest Norian to early Rhaetian age (López- Gómez *et al*. 1998).

In the studied area (Figs. 2 and 3) the upper part of the Keuper facies is further subdivided into three parts (lower, middle, upper); magmatic bodies are only recognised in the middle part.

The lower part is relatively simple and shows similar features in both sectors (Cameros and Moncayo). This sequence is formed by units of red-orange compact argillites of variable thickness (up to 20 m), interbedded with siltstones and dolomite-limestone beds of cm-scale thickness (Fig. 3A and B).

The middle part is formed by a magmatic-sedimentary sequence. It is composed of several igneous layers emplaced into argillites. The thickness of this part increases from the SE (5-50 m in the Moncayo sector) to the NW (30-100 m in the Cameros sector) (Fig. 3a and b). Only one igneous unit is recognised in the Moncayo sector, whereas several igneous units crop out in the Cameros sector.

The upper part shows marked differences in the two studied sectors. In the Cameros sector (Fig. 3a) it is generally formed by a relatively thin (1 to 7 m) sequence of marly-argillites to marls and dolomite-limestone units. In the Moncayo sector (Fig. 3b) it comprises argillites, siltstones and sandstones. The sandstones consist of cm- to dm-scale beds of fine to medium grain-size with planar-cross-bedding. Characteristically, different (up to 5) decimetric beds of conglomerate are recognised within the argillite units. These conglomerates include angular to

sub-rounded heterometric clasts of igneous rocks, dolomites, argillites and quartzites (Fig. 4a), showing a main grain-supported texture and a vertical grain-size decrease. The clasts of igneous rocks are petrologically similar to the igneous bodies emplaced in the middle part (Lago *et al.*, 1996). In most cases, the conglomerate beds show a lenticular to tabular geometry with channel-shaped basal surfaces of SW-NE main direction. The thickness of the conglomerate beds and the size of the clasts decrease to the SE, where comprises a decimetric microconglomeratic bed near Arándiga, within marly-argillites and centimetric dolomite beds (sections 15-17; Fig. 3b); in this case the clasts are homometric and subrounded to rounded in shape. The upper part of the Keuper facies in the Moncayo sector reaches its maximum thickness (12 m) in the western part, except for section 11 (Figs. 2 and 3b) where it is absent.

Concerning the Imón Fm, in the Cameros sector it comprises a lower part of massive grey dolomites and an upper part of dolostone breccias (Fig. 3a). In contrast, in the Moncayo sector it is preceded by a metric sequence of yellowish marls or marly-limestones with centimetric layers of interbedded massive vuggy dolostones. The Imón Fm is sometimes not present, as in the case of section 15, where the basal Lower Jurassic deposits directly overlie the Keuper facies (Fig. 3b).

3. Field description

The studied outcrops are oriented along a NW-SE trend of cartographic scale (Fig. 2). The outcrops of the Cameros sector are located in the north-eastern part of the Cameros massif, close to the alpine North Cameros thrust front. On the other hand, the outcrops of the Moncayo sector are located near to the NW–SE Tablado-Jarque fault.

The igneous levels are grey coloured, with a purple hue at the most altered areas. They are usually concordant with the stratification and present two main directions: NNW-SSE and W-E, related to their location at the flanks

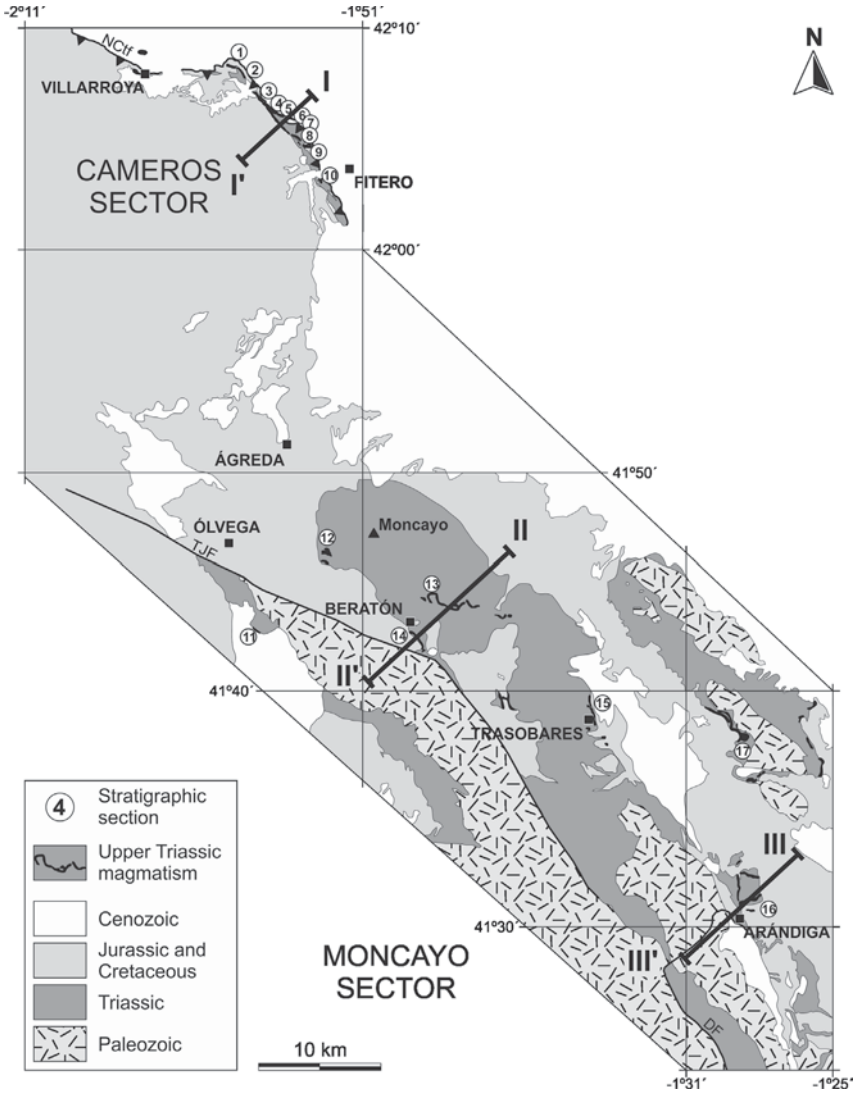

Fig. 2.- Synthetic geological map of the studied sectors. The numbers indicate the location of the studied stratigraphic sections (Fig. 3). NCtf: North Cameros thrust front; TJF: Tablado-Jarque Fault; DF: Datos Fault. The lines indicate the location of the cross sections in Fig. 11. Modified from the MAGNA cartography, sheets n. 281, 319, 320, 351, 352, 353, 381, 382, 409 and 410.

Fig. 2.- Mapa geológico de síntesis de los sectores estudiados. Los números indican la localización de los perfiles estratigráficos estudiados (Fig. 3). NCtf: Frente norte de Cabalgamiento de Cameros; TJF: Falla Tablado-Jarque; DF: Falla de Datos. Las líneas indican la localización de los cortes geológicos de la Fig. 11. Modificado a partir de la cartografía MAGNA, hojas n. 281, 319, 320, 351, 352, 353, 381, 382, 409 y 410.

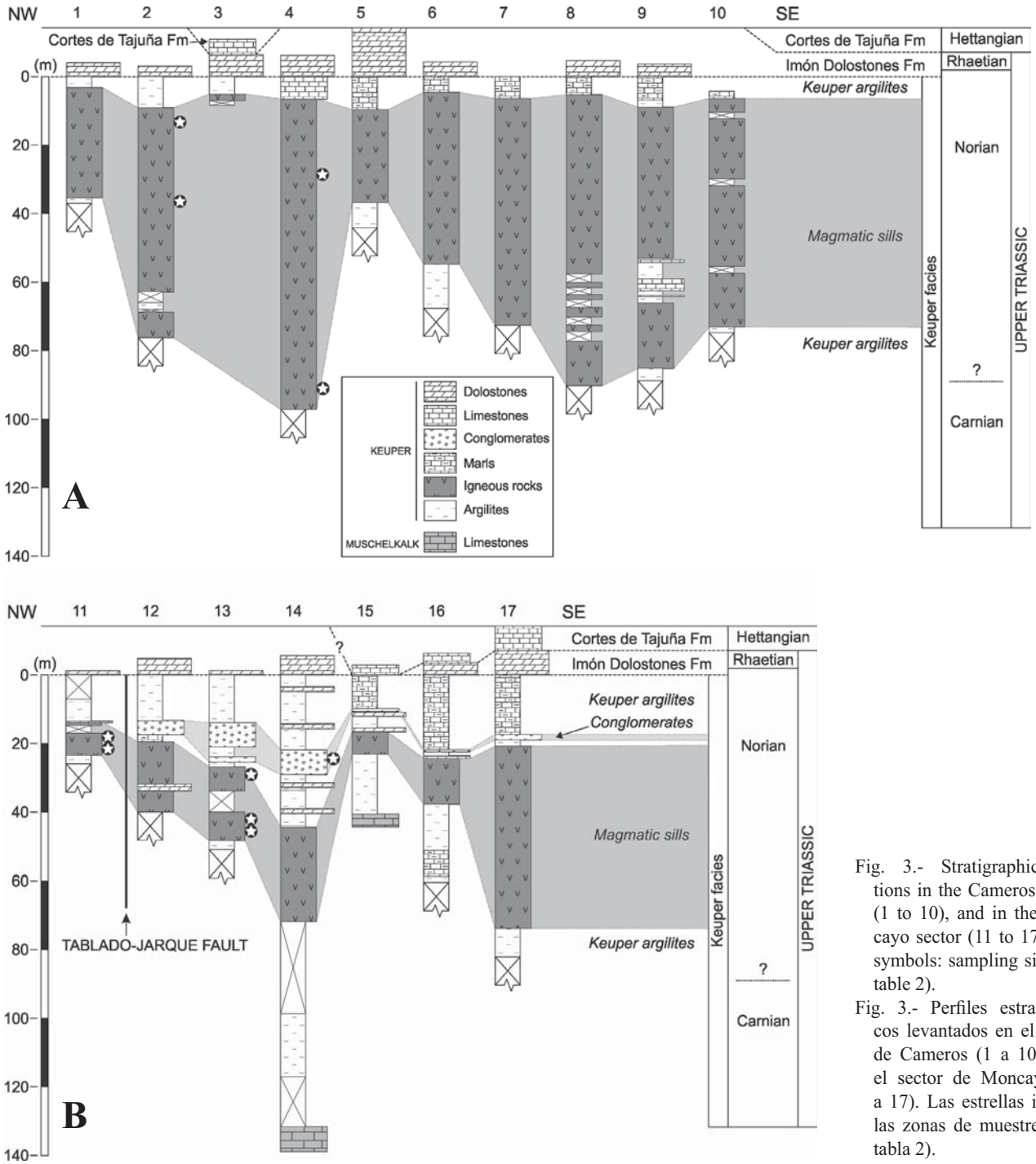

Fig. 3.- Stratigraphic sections in the Cameros sector (1 to 10), and in the Moncayo sector (11 to 17). Star symbols: sampling site (see table 2).

Fig. 3.- Perfiles estratigráficos levantados en el sector de Cameros (1 a 10) y en el sector de Moncayo (11 a 17). Las estrellas indican las zonas de muestreo (ver tabla 2).

of a main alpine fold of NW-SE axis orientation (Fig. 2).

Ten sections have been studied in the Cameros sector (Fig. 3a). The igneous levels show a tabular to irregular shape, although some folded bodies have been observed as well. The thickness of the igneous levels varies from 2 to 69 m. The number of levels recognised in each section also varies; up to three levels, separated by centimetric beds of argillites, have been recognised in the central and the southeastern part of this sector. The maximum thickness of exposed igneous rocks reaches up to 94 m in the central part of the Cameros Massif (section 4; Fig. 3a).

Seven stratigraphical sections have been studied in the Moncayo sector (Fig. 3b). In this area only one igneous body crops out per section. The igneous body is thinner (0.6 to 38 m) than the igneous bodies of the Cameros sector. The maximum thickness (38 m) corresponds to the eastern part of the Moncayo Massif (section 17; Fig. 3b).

In detail, the contact between the igneous bodies and the sedimentary host-rocks is generally irregular and characterised by a transition zone from the igneous rock to the sedimentary rock. This zone is composed of cm-scale sub-rounded igneous rocks intermixed with the

host-rock sediments (Fig. 4b). These structures are considered peperites as defined by White *et al*. (2000) and Skilling *et al*. (2002). Besides, sediment injections and irregular cm-scale fragments of structure-less sediments are locally observed inside the intrusions (Fig. 4c), close to their lower margin. Furthermore, a low-grade contact metamorphism has been identified in the sedimentary host-rocks at the Moncayo sector (Bastida *et al*., 1989).

Vesicles are frequent in the igneous rocks. They are rounded or elongated in shape, millimetric to centimetric in size and filled by calcite and quartz (Fig. 4d). In most cases, several vesicle-rich levels can be identified, oriented parallel to the contact with the host-rock.

The igneous bodies are heterogeneous and a petrological zoning can be usually established from the margin to the centre (Bastida *et al.*, 1989): a) chilled margin facies, b) central facies and c) pegmatoid facies. The chilled margin facies includes dark-grey coloured aphanitic rocks with common vesicle-rich levels (Fig. 4d) and xenoliths. The central facies includes light-grey coloured massive igneous rocks with non oriented mm-sized phenocrysts, visible to the naked eye; most of them are black-coloured, olivine crystals (Fig. 4e). The pegmatoid facies is developed locally in the innermost areas of the intrusions. It consists of light grey, cm- to dm-scale levels which include bigger crystals than those in the central facies, up to centimetric in diameter (Fig. 4f).

In the Cameros domain, the vertical zoning of the igneous bodies is not always consistent. As explained above, the chilled margin facies is usually located at the margins and the central facies represents the centre of the igneous bodies. However, we have identified several examples where the sequence chilled margin – central facies is repeated several times, so that chilled margins are also recognised at the centre of the bodies (e.g. section 2, Fig. 3a). In other sections mechanical contacts (fault breccias composed of igneous and host-rock clasts) have been identified between different zones of the central facies (e.g. section 7, Fig. 3a).

4. Samples and methods

The stratigraphical study of the magmatism has been undertaken through 17 stratigraphic sections (1-17; Fig. 2 and 3). They are focused on the igneous rocks and include the sedimentary units over and below them as well, recording the Triassic – Jurassic transition in the study area: from the Upper – Triassic (Carnian) argillitic beds, to the Imón Fm (latest Norian to early Rhaetian; López Gómez *et al*., 1998). Both the igneous and the sedimentary units have been studied in detail.

More than 300 rock samples were collected from the studied stratigraphic sections. They are strongly affected by spilisation that triggers alteration of the primary mineral assemblage and mobilisation of H_2O, CO_2, Li, Rb, Sr, Ba, K and Cu (e.g. Cabral and Beaudoin, 2007; Lago *et al*., 1996 and references therein; Shaw *et al*., 1977). After careful petrographical examination of the rocks, the 53 least altered samples were selected for mineral and whole rock analyses.

Mineral compositions were determined on 30 μm thick polished sections by electron microprobe (EMPA) at the *Centro de Nacional Microscopía Electronica* of the Complutense University (Madrid, Spain), using a JEOL JZA-8900 M electron microprobe equipped with four wavelength dispersive spectrometers. Analyses were performed using an accelerating voltage of 15 kV and an electron beam current of 20 nA, with a beam diameter of 5 μm. Elemental counting times were 10 s on the peak and 5 s on each of two background positions. Analyses were corrected for electronic interactions using a ZAF procedure (atomic number (Z), absorption (A) and fluorescence (F)).

The samples selected for whole rock analyses were crushed in a manganese steel jaw-crusher and milled in an agate vibrating cup mill at the *Servicios de Apoyo a la Investigación* of the University of Zaragoza (Spain). Major and trace element concentrations were determined at the *Service d´Analyse des Roches et des Minéraux (SARM)* in Nancy (France) and the *XRAL Laboratories* (Canada). The samples were analysed by ICP-AES for major elements and ICP-MS for trace elements. Details on the analytical procedures and detection limits are available at *http://helium.crpg.cnrs-nancy.fr/SARM/pages/roches.html.* The geochemical classification and the stratigraphic position of the selected samples are summarised in Table 2.

Data treatment was undertaken with "ad-hoc" built spreadsheets. Mineral abbreviations in the figures and the tables follow recommendations by Whitney and Evans (2010).

5. Petrography

The above described three igneous facies, defined on the basis of their field appearance, show also systematic differences under the petrographic microscope. The chilled margin facies is composed of plagioclase (50 vol. %), opaque minerals (10 vol. %) and pseudomorphed olivine (7-8 vol. %); some olivine-rich samples (up to 10 vol. %) have been recognised in the Cameros sector. This facies is vesicle-rich (30-35 vol. %); the vesicles are filled by quartz and calcite. The microstructure of this facies is aphyric to porphyritic (Fig. 5a), defined by large (up to 1.9 mm) subidiomorphic crystals of olivine replaced by secondary calcite, chlorite and opaque minerals, set in a finer-grained groundmass (150 – 250 μm). The micro-

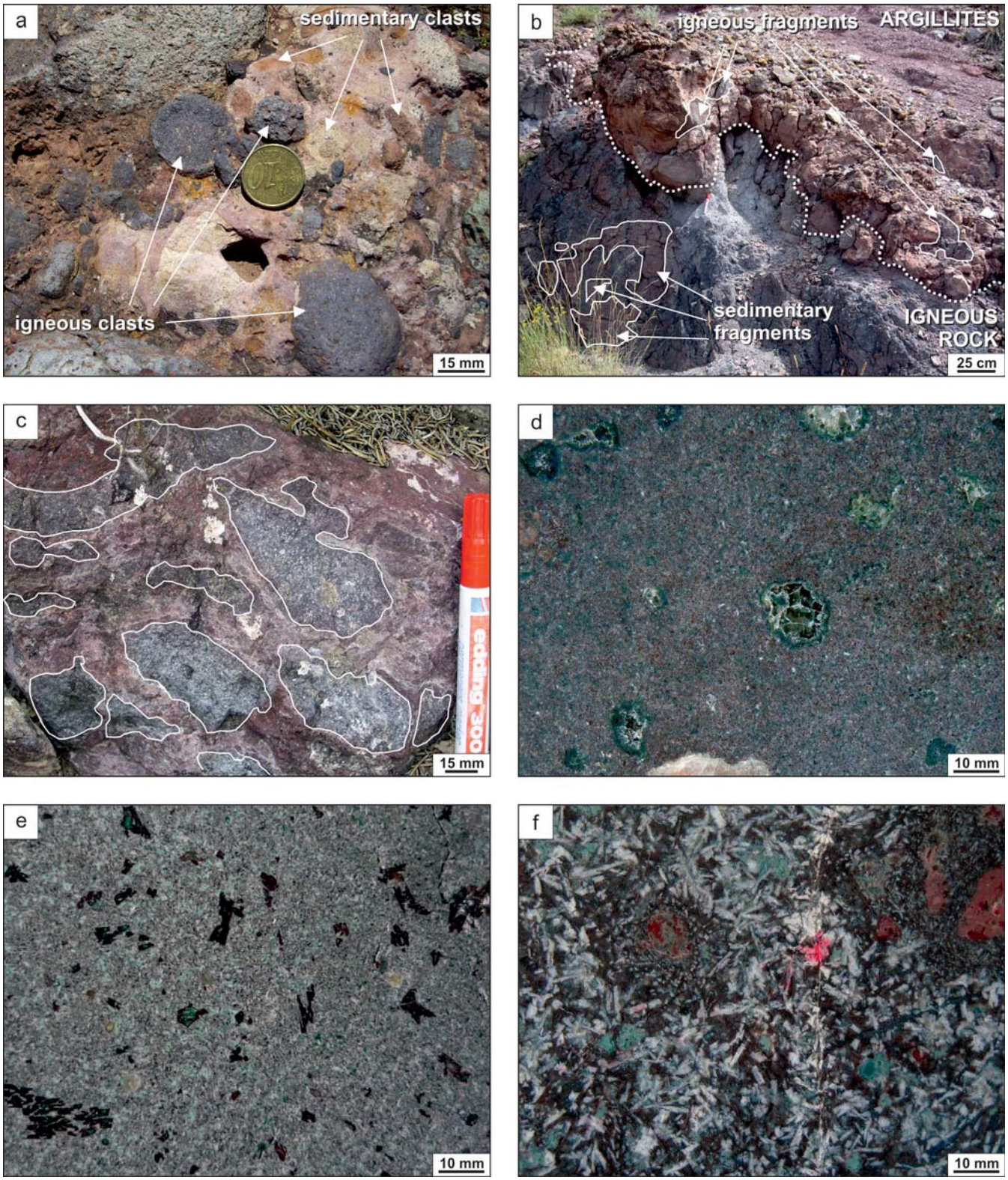

Fig. 4.- Field photographs of the studied outcrops. a- Conglomerate with igneous clasts similar to the studied igneous rocks. b- Irregular contact between the sill and the host-sedimentary rock showing sub-rounded igneous rocks intermixed with the host-rock sediments. c- Irregular cm-scale fragments of structure-less sediments observed inside the intrusions. d- Vesicle-rich, aphanitic chilled margin. e- Central facies with non oriented mm-sized olivine phenocrysts, visible to the naked eye. f- Pegmatoid facies.

Fig. 4.- Fotografías de campo de los afloramientos estudiados. a- Conglomerado con clastos ígneos similares a las rocas ígneas estudiadas. b- Contacto irregular entre el sill y su roca sedimentaria encajante, mostrando fragmentos subredondeados de roca ígnea mezclada con el sedimento encajante. c- Fragmentos centimétricos irregulares de sedimentos sin estructura interna, reconocidos en el interior de las intrusiones. d- Roca afanítica y rica en vesículas de la facies de borde enfriado. e- Roca de la facies central, con fenocristales milimétricos, no orientados, de olivino, visibles a simple vista. f- Roca de la facies pegmatoide.

crysts of the groundmass (mainly plagioclase and opaque minerals) are widely altered to calcite and chlorite. Several xenoliths of the sedimentary host-rock (up to 15 mm in size) have been observed. They have a 100 – 300 μm thick brown glassy rim which contains microlites of plagioclase and abundant oxides (Fig. 5b).

The central facies (Fig. 5c) is composed of plagioclase (65-70 vol. %), pseudomorphed olivine (15 vol. %), clinopyroxene (5 vol. %) and opaque minerals (5 vol. %). It shows a porphyritic to doleritic microstructure with subidiomorphic large crystals of olivine (up to 1.6 mm). The rock groundmass (7 vol. %) is composed of microcrysts of plagioclase, clinopyroxene and opaque minerals; secondary chlorite and calcite are common. Vesicles are uncommon in this facies and no xenoliths are observed.

The pegmatoid facies shows an equigranular microstructure with subidiomorphic crystals up to 1200 μm (Fig. 5d). It is composed of plagioclase (75-80 vol. %), opaque minerals (10-15 vol. %), pseudomorphed olivine (5-10 vol. %) and accessory apatite.

6. Geochemistry

6.1. Mineral chemistry

Mineral compositions were determined for feldspar (Table 1), clinopyroxene (Table 1), opaque minerals and apatite. Olivine crystals are completely replaced by secondary minerals, so their original composition could not be determined.

Feldspar was analysed in samples from the central facies and the pegmatoid; in the latter, plagioclase is albitised and K-feldspar is also recognised. On the other hand, feldspar from the central facies is classified as plagioclase, with compositions ranging from labradorite to anorthoclase (An_{64-14} Ab_{34-73} Or_{01-12}; Table 1; Fig. 6a). The analysed compositions display a typically alkaline trend of increasing orthose with decreasing anorthite (Fig. 6a).

Clinopyroxene is only present in the central facies. All the compositions are classified as Al-rich augite (Wo_{43-39} En_{49-39} Fs_{12-22}), according to Morimoto *et al*. (1988); they are moderately rich in Cr_2O_3 (up to 0.58 wt. %) and TiO_2 (up to 1.62 wt. %). The results define poor correlation trends with fractionation, represented by the decrease in mg* [mg* = Mg / (Mg+Fe^{2+}+Fe^{3+}+Mn)] per formula unit, p.f.u., where Fe^{3+} is calculated according to Droop (1987). SiO_2, Al_2O_3, CaO and Cr_2O_3 decrease with decreasing mg*, whereas TiO_2 increases with decreasing mg*. Na_2O displays a significant scatter of the values. The compositions plot between the alkaline and the subalkaline fields defined by Leterrier *et al*. (1982; Fig. 6b).

Opaque minerals are classified as ilmenite. Their compositions vary from 55.45 to 66.19 wt. % TiO_2 and from 33.81 to 44.55 wt. % FeO_T. Apatite was only analysed in the Moncayo sector and is F-rich; its composition varies from 40.10 to 42.06 wt. % P_2O_5 and from 52.56 to 54.80 wt. % CaO.

Mineral	Pl				Cpx			
Type	rim	core	rim	core	core	>	>	rim
SiO_2	64.13	52.76	64.78	63.05	51.77	51.37	50.51	50.87
TiO_2	0.16	0.07	0.07	0.11	1.29	1.51	1.54	1.51
Al_2O_3	21.40	29.90	21.59	22.55	2.68	2.36	2.23	1.45
Cr_2O_3	n.a.	n.a.	n.a.	n.a.	0.58	0.13	0.07	0.05
MgO	0.54	0.15	0.22	0.05	15.77	15.43	14.69	13.45
FeO_t	0.57	0.49	0.49	0.57	7.58	9.89	11.59	13.43
NiO	0.00	0.01	0.00	0.05	0.05	0.05	0.05	0.03
MnO	0.00	0.00	0.00	0.00	0.09	0.14	0.15	0.17
CaO	3.22	12.52	3.01	4.17	20.00	19.01	18.42	18.96
Na_2O	7.08	4.20	8.47	8.08	0.29	0.26	0.32	0.26
K_2O	3.88	0.27	2.19	2.01	0.00	0.00	0.01	0.00
BaO	0.00	0.00	0.00	0.00	n.a.	n.a.	n.a.	n.a.
Total	100.98	100.37	100.82	100.64	100.10	100.15	99.58	100.18
Si	2.84	2.39	2.86	2.80	1.91	1.91	1.90	1.92
Ti	0.01	0.00	0.00	0.00	0.04	0.04	0.04	0.04
Al	1.12	1.59	1.12	1.18	0.12	0.10	0.10	0.06
Cr	--	--	--	--	0.02	0.00	0.00	0.00
Fe^{3+}	--	--	--	--	0.00	0.00	0.03	0.02
Mg	0.04	0.01	0.01	0.00	0.87	0.85	0.82	0.76
Fe^{2+}	--	--	--	--	0.23	0.30	0.33	0.41
Fe^t	0.02	0.02	0.02	0.02	--	--	--	--
Ni	0.00	0.00	0.00	0.00	0.00	0.00	0.00	0.00
Mn	0.00	0.00	0.00	0.00	0.00	0.00	0.00	0.01
Ca	0.15	0.61	0.14	0.20	0.79	0.76	0.74	0.77
Na	0.61	0.37	0.72	0.70	0.02	0.02	0.02	0.02
K	0.22	0.02	0.12	0.11	0.00	0.00	0.00	0.00
Ba	0.00	0.00	0.00	0.00	--	--	--	--
Total	5.0	5.0	5.0	5.0	4.0	4.0	4.0	4.0
An	16	61	14	20	--	--	--	--
Ab	62	37	73	69	--	--	--	--
Or	22	2	12	11	--	--	--	--
En	--	--	--	--	46	44	43	39
Fs	--	--	--	--	13	16	19	22
Wo	--	--	--	--	42	39	38	39
mg#	--	--	--	--	79	73	69	64

Table 1.- Representative major element composition (expressed as wt.%) of minerals from the studied igneous rocks. Structural formulae calculated to 8 (Pl) and 6 (Cpx) oxygens. Fe^{3+} was calculated using Droop (1987) algorithm.

Tabla 1.- Composiciones en elementos mayores representativas (expresadas en % en peso) de minerales de las rocas ígneas estudiadas. Fórmula estructural calculada a 8 (Pl) y 6 (Cpx) oxígenos. Fe^{3+} calculado mediante el algortimo de Droop (1987).

6.2. Whole-rock chemistry

All the selected samples from the Cameros and Moncayo sectors are affected by spilitisation (Lago *et al*., 1989) and show variable LOI (Loss On Ignition) contents, ranging from 3.17 to 8.51 wt. % (Table 2).

The rocks of the chilled margins and the central facies are classified as tephrites, basalts, basaltic andesites

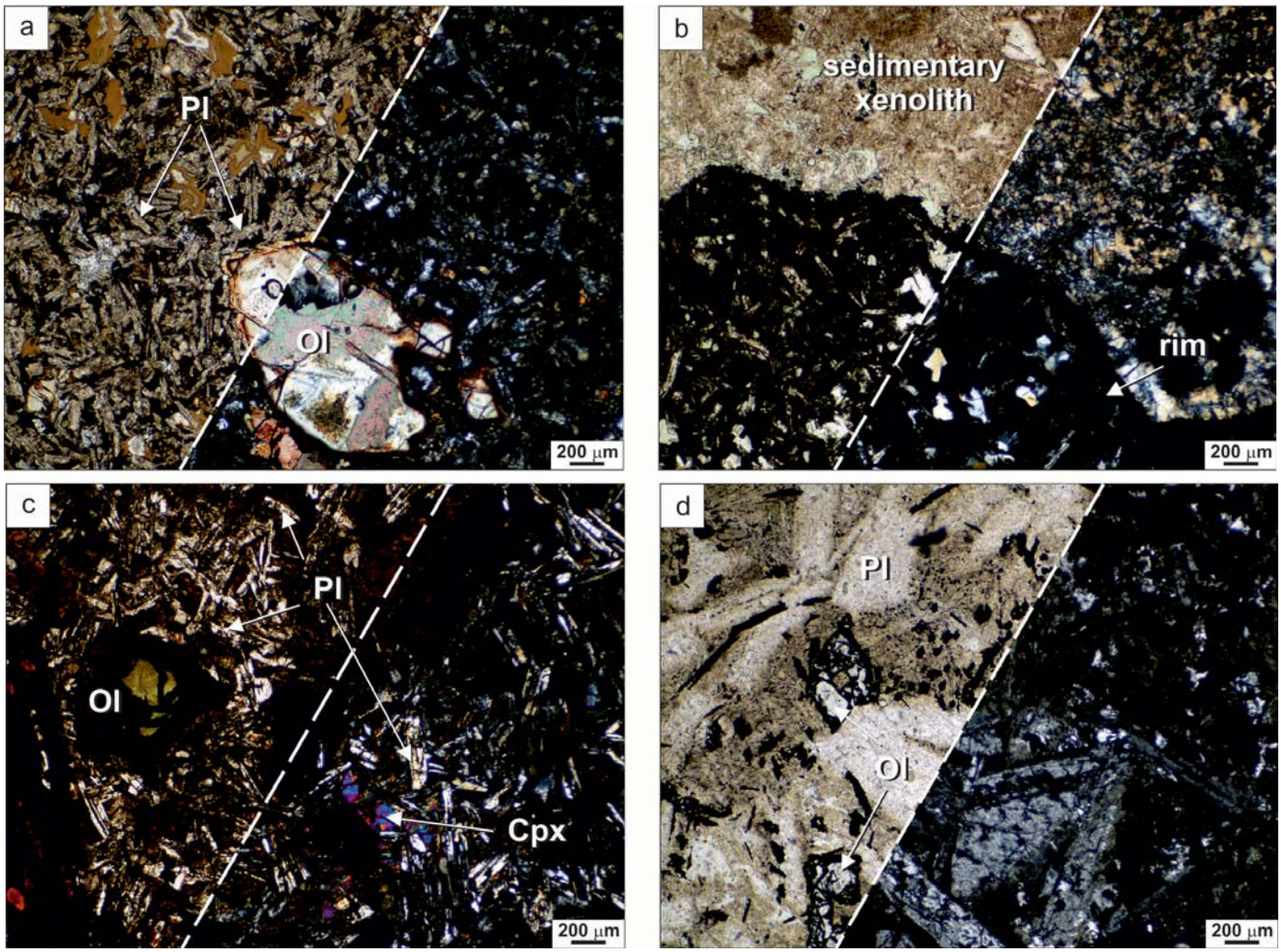

Fig. 5.- Thin section photomicrographs (plane- and cross-polarised transmitted light). Mineral abbreviations follow recommendations by Whitney and Evans (2010). a- Porphyritic microstructure of the chilled margin facies defined by large subidiomorphic crystals of olivine replaced by secondary calcite, chlorite and opaque minerals, set in a finer-grained groundmass (mainly composed of plagioclase and opaque minerals). b- Xenolith of the sedimentary host-rock with a thick brown glassy rim which contains microlites of plagioclase and abundant oxides. c- Porphyritic to doleritic microstructure of the central facies, defined by large crystals of pseudomorphed olivine and a rock groundmass composed of plagioclase, clinopyroxene and opaque minerals. d- Equigranular to intersertal microestructure of the pegmatoid facies composed of plagioclase, opaque minerals and pseudomorphed olivine.

Fig. 5.- Microfotografías en lámina delgada (luz transmitida, en nícoles paralelos y cruzados). Las abreviaturas de minerales siguen la terminología propuesta de Whitney y Evans (2010). a- Textura porfídica de la facies de borde enfriado, definida por grandes pseudomorfos de olivino en una mesostasia compuesta de plagioclasa y opacos. b- Xenolito de roca sedimentaria encajante que presenta un borde vítreo con microlitos de plagioclasa y abundantes minerales opacos. c- Textura porfídica a dolerítica de la facies central, definida por grandes cristales de olivino pseudomorfizados y una mesostasia formada por plagioclasa, clinopiroxeno y minerales opacos. d- Textura equigranular a intersertal de la facies pegmatoide, definida por plagioclasa, minerales opacos y olivino pseudomorfizado.

and shoshonites whereas the pegmatoid facies includes the most evolved rocks: andesites and dacites (Fig. 7a). According to the Zr/TiO_2 vs. Nb/Y diagram for altered rocks (Winchester and Floyd, 1977), most samples are classified as alkali basalts, but four of them are classified as subalkali basalts (Fig. 7b). According to the CIPW norm, the samples are plagioclase-, orthoclase-, apatite- and hypersthene-normative; most of them are also quartz-normative except for the tephrites which are olivine-normative. These results agree with the high modal proportion of plagioclase and silica contents of the rocks.

The SiO_2 content varies from 41.40 wt. % in the most primitive rocks to 61.60 wt. % in the most evolved ones. The chilled margins and central facies show similar SiO_2 concentrations (41.40–53.51 wt. %), which fits well with basic to intermediate rocks. Accordingly, these samples have relatively high MgO contents (15.04–7.19 wt. %; mg#: 0.77–0.58, where mg# = MgO/(MgO+FeO)). In contrast, the pegmatoid facies comprises more evolved rocks (54.50-61.60 wt. % SiO_2) and with lower MgO contents (8.15–5.60 wt. %; mg#: 0.66–0.54). None of the analysed samples (Table 2) presents compositional

Referencia	281-4-C3	281-1-C9	281-1-D2	281-1-F2	FIT-X	AGR-P	AGR-7	AGR-23	281-4-C1
Rock Type	Bas And	Bas And	Bas And	And	Bas And	Teph	Bas And	Shos	Bas And
Facies	Cen	Cen	Cen	Cen	Cen	Cen	Cen	Cen	Bor
Section	out	2	2	3	9	11	11	11	out
SiO_2	51.90	50.60	52.20	53.20	52.08	41.43	53.00	50.50	50.40
TiO_2	1.63	1.63	1.67	1.41	2.35	1.84	1.45	1.57	1.61
Al_2O_3	14.07	15.36	14.66	14.72	12.84	14.96	15.05	14.33	12.75
Fe_2O_3	10.42	8.62	8.48	8.23	9.16	11.27	7.91	10.41	11.00
MnO	0.02	0.03	0.05	0.03	0.02	0.02	0.02	0.03	0.02
MgO	10.50	7.63	7.19	10.30	8.08	11.36	10.75	8.96	15.04
CaO	1.12	5.85	5.82	1.69	2.99	3.40	0.86	1.80	0.55
Na_2O	0.17	2.30	2.52	2.86	2.73	0.08	2.98	1.87	0.12
K_2O	4.44	1.07	1.19	1.41	2.00	6.45	2.04	4.48	1.91
P_2O_5	0.34	0.40	0.43	0.37	0.32	0.26	0.30	0.35	0.48
LOI	5.62	5.94	5.76	6.81	6.59	7.90	5.11	5.00	6.96
mg*	0.70	0.67	0.66	0.74	0.67	0.70	0.76	0.66	0.76
TOTAL	100.23	99.43	99.97	101.03	99.15	98.96	99.47	99.30	100.84
Li	125	52	62	372	n.a	n.a.	142	76	192
Rb	54	13	20	10	23	68	21	54	17
Cs	n.a.	n.a.	n.a.	n.a.	0	0	0	0	n.a.
Be	n.a.	n.a.	n.a.	n.a.	1	1	0	0	n.a.
Sr	25	247	292	105	126	42	48	75	11
Ba	166	158	219	215	311	223	140	350	50
Sc	22	22	20	20	n.a	n.a.	23	23	17
V	173	207	187	187	182	265	173	204	181
Cr	211	216	240	227	141	281	197	258	220
Co	50	64	60	55	29	37	56	57	57
Ni	134	157	154	149	104	140	134	156	148
Cu	8	29	16	30	6	7	6	6	7
Zn	29	42	40	140	22	22	27	25	30
Ga	19	16	19	19	16	17	20	19	17
Y	10	17	18	15	25	17	14	14	9
Nb	8	14	19	13	19	15	8	9	17
Ta	n.a.	n.a.	n.a.	n.a.	1.4	1.1	n.a.	n.a.	n.a.
Zr	23.0	89.0	119.0	51.0	156.5	122.6	21.0	24.0	14.0
Hf	n.a.	n.a.	n.a.	n.a.	3.99	3.13	n.a.	n.a.	n.a.
Mo	n.a.	n.a.	n.a.	n.a.	1.47	0.88	n.a.	n.a.	n.a.
Sn	n.a.	n.a.	n.a.	n.a.	1.68	1.34	n.a.	n.a.	n.a.
Tl	n.a.	n.a.	n.a.	n.a.	0.00	n.a.	n.a.	n.a.	n.a.
Pb	n.a.	n.a.	n.a.	n.a.	2.60	1.93	n.a.	n.a.	n.a.
U	0.50	0.50	0.90	0.90	1.02	2.49	0.50	0.60	2.60
Th	1.20	1.90	2.50	1.50	2.64	1.99	1.10	1.10	1.90
La	12.90	12.10	16.90	9.90	13.30	7.25	7.20	9.60	6.90
Ce	26.50	24.80	33.00	21.00	28.68	15.35	17.20	20.40	13.70
Pr	3.50	3.10	4.10	2.80	3.78	2.13	2.50	2.90	1.70
Nd	17.50	14.50	19.20	13.80	16.70	9.68	11.40	14.00	8.50
Sm	4.10	3.50	3.90	3.40	4.41	2.86	3.40	3.70	2.70
Eu	1.14	1.12	1.42	0.76	1.25	0.87	0.99	1.41	0.95
Gd	3.40	3.30	4.10	3.60	4.78	3.18	3.70	3.70	2.90
Tb	0.50	0.50	0.60	0.50	0.79	0.53	0.60	0.60	0.50
Dy	2.30	2.90	3.30	2.80	4.78	3.15	3.00	3.30	2.10
Ho	0.36	0.60	0.62	0.52	0.93	0.62	0.50	0.54	0.37
Er	0.90	1.70	1.80	1.50	2.47	1.72	1.40	1.40	1.00
Tm	0.10	0.20	0.20	0.20	0.36	0.25	0.10	0.10	0.10
Yb	0.60	1.10	1.30	1.00	2.23	1.65	0.70	0.80	0.60
Lu	0.09	0.20	0.20	0.15	0.32	0.25	0.09	0.11	0.08
Nb/Y	0.80	0.82	1.06	0.87	0.76	0.86	0.57	0.64	1.89
(La/Yb) n	14.55	7.45	8.80	6.70	4.03	2.98	6.96	8.12	7.78
(La/Sm) n	1.98	2.18	2.73	1.84	1.90	1.60	1.34	1.64	1.61
Ti/V	56	47	54	45	77	42	50	46	53

Table 2.- Major element (wt.%) and trace element (ppm) composition of selected samples from studied igneous rocks.
Tabla 2.- Composición en elementos mayores (% en peso) y traza (ppm) de muestras seleccionadas de las rocas ígneas estudiadas.

features typical of primitive magmas in equilibrium with their mantle source (which typically show MgO > 11 wt. %, Cr > 500-1000 ppm and Ni > 200–500 ppm; Frey *et al*., 1978).

The variability in whole-rock major element abundances is illustrated using MgO variation diagrams (Fig. 8). Generally, there is a wider scatter of major element distributions. However, some poor correlations can be estab-

Referencia	281-1-TS1	CAV-2	AGR-1	AGR-3	AGR-28	352-3-20	BER-1	AGR-13	352-3-I2	352-3-I6
Rock Type	Bas And	Shos	Bas And	Bas	Shos	Teph	Teph	Bas And	Dac	And
Facies	Bor	Bor	Bor	Bor	Bor	Bor	Bor	Pegm	Pegm	Pegm
Section	3	11	11	11	11	13	14	11	13	13
SiO_2	49.62	53.51	51.00	48.00	51.50	41.40	44.77	54.50	61.60	57.40
TiO_2	1.69	1.39	1.65	1.43	1.56	1.96	1.93	2.51	3.32	3.00
Al_2O_3	14.76	12.83	12.93	13.30	14.60	14.30	14.97	11.37	11.80	12.59
Fe_2O_3	7.36	13.87	8.54	14.22	7.64	16.54	10.13	13.75	6.65	10.34
MnO	0.02	0.02	0.04	0.03	0.03	0.02	0.01	0.02	0.01	0.12
MgO	11.04	8.53	10.27	11.68	11.41	13.55	10.23	7.05	5.60	8.15
CaO	2.65	0.46	2.96	0.50	1.09	0.83	3.09	0.97	0.91	0.89
Na_2O	1.89	0.29	1.78	0.82	0.78	1.54	0.06	3.62	2.00	2.70
K_2O	2.10	5.61	2.38	3.42	4.95	3.72	6.58	1.91	4.20	1.00
P_2O_5	0.27	0.19	0.44	0.35	0.26	0.39	0.34	0.68	0.42	0.44
LOI	8.51	4.34	7.51	5.67	6.01	5.94	7.20	3.98	3.17	3.30
mg*	0.77	0.58	0.73	0.65	0.77	0.65	0.70	0.54	0.66	0.64
TOTAL	99.91	101.03	99.50	99.42	99.83	100.19	99.32	100.36	99.68	99.93
Li	n.a	n.a.	150	140	131	124	n.a.	68	80	73
Rb	25	55	26	33	50	46	56	22	45	41
Cs	1	0	n.a.	n.a.	n.a.	n.a.	0	0	0	0
Be	1	1	n.a.	n.a.	n.a.	n.a.	0	0	0	0
Sr	76	25	37	21	18	21	53	84	68	53
Ba	174	200	165	134	145	181	210	146	264	250
Sc	n.a	n.a.	21	20	22	19	n.a.	18	18	20
V	179	149	217	188	175	246	212	188	202	198
Cr	278	218	207	172	201	244	599	33	32	155
Co	29	35	56	61	57	52	33	60	54	82
Ni	143	138	130	170	140	166	121	107	90	347
Cu	6	6	7	9	5	10	22	42	10	150
Zn	140	23	21	34	27	26	32	32	18	117
Ga	20	16	18	19	20	21	17	18	14	13
Y	20	20	18	13	14	10	19	13	12	14
Nb	19	9	15	10	10	10	14	7	19	22
Ta	1.4	0.6	n.a.	n.a.	n.a.	n.a.	0.9	n.a.	n.a.	n.a.
Zr	131.2	86.2	18.0	30.0	20.0	16.0	113.7	23.0	29.0	37.0
Hf	3.26	2.27	n.a.	n.a.	n.a.	n.a.	3.00	n.a.	n.a.	n.a.
Mo	0.84	0.79	n.a.	n.a.	n.a.	n.a.	0.98	n.a.	n.a.	n.a.
Sn	1.62	1.13	n.a.	n.a.	n.a.	n.a.	1.41	n.a.	n.a.	n.a.
Tl	n.a.	n.a.	n.a.	n.a.	n.a.	n.a.	n.a.	n.a.	n.a.	n.a.
Pb	1.56	1.11	n.a.	n.a.	n.a.	n.a.	0.94	n.a.	n.a.	n.a.
U	1.21	2.02	1.90	2.00	0.50	1.90	3.43	0.30	1.90	2.30
Th	2.93	1.66	1.90	1.70	1.00	2.70	1.85	1.50	2.60	3.00
La	11.23	5.98	14.00	8.40	4.80	14.00	7.06	15.30	17.50	31.90
Ce	24.19	12.63	27.30	18.20	14.20	26.80	13.86	30.50	34.00	61.80
Pr	2.97	1.73	3.70	2.40	2.70	3.60	2.14	4.30	4.60	8.10
Nd	12.53	7.90	17.40	12.10	16.00	16.10	10.01	20.20	21.30	36.60
Sm	3.03	2.70	4.40	4.20	4.90	4.30	3.32	4.90	5.10	8.00
Eu	0.80	0.95	1.36	1.28	1.98	1.29	0.91	1.43	1.31	1.94
Gd	3.31	3.47	5.00	4.60	4.70	4.40	3.85	4.30	5.00	6.40
Tb	0.58	0.62	0.80	0.70	0.70	0.60	0.60	0.60	0.60	0.80
Dy	3.73	3.83	4.10	3.20	3.50	3.10	3.45	3.00	3.20	3.30
Ho	0.73	0.74	0.71	0.52	0.53	0.48	0.63	0.52	0.50	0.52
Er	1.93	1.99	1.90	1.50	1.30	1.30	1.63	1.30	1.10	1.40
Tm	0.27	0.28	0.20	0.20	0.10	0.20	0.22	0.20	0.20	0.10
Yb	1.67	1.75	1.10	0.90	0.70	0.70	1.32	0.80	0.80	0.80
Lu	0.24	0.26	0.14	0.12	0.08	0.09	0.19	0.09	0.09	0.10
Nb/Y	0.98	0.44	0.83	0.77	0.71	1.00	0.73	0.54	1.58	1.57
(La/Yb) n	4.56	2.32	8.62	6.32	4.64	13.54	3.61	12.95	14.81	26.99
(La/Sm) n	2.34	1.40	2.01	1.26	0.62	2.05	1.34	1.97	2.16	2.52
Ti/V	56	56	46	46	53	48	55	80	99	91

Table 2.- Cont.
Tabla 2.- Cont.

lished. Fe_2O_3t behaves compatibly and shows a decrease in abundance with the decreasing MgO (Fig. 8), whereas SiO_2, TiO_2, and Na_2O increase with the decreasing of MgO (Fig. 8). Al_2O_3, MnO, CaO, K_2O and P_2O_5 abundances are relatively constant or scatter at varying MgO contents (not shown). LOI values are higher in the chilled margins and central facies, probably related to the high alteration degree shown by olivine and clinopyroxene crystals. Fig.

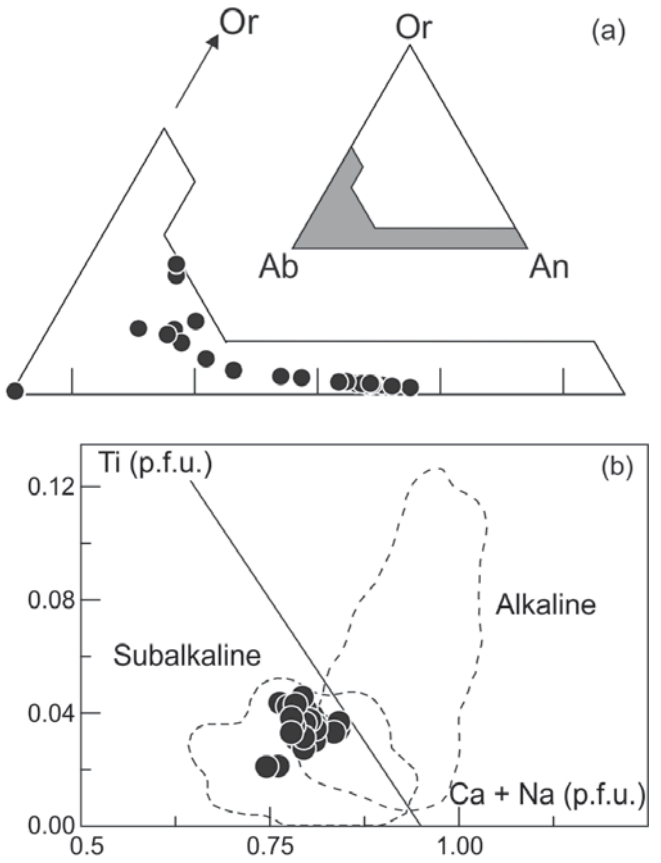

Fig. 6.- Mineral composition of the studied sills. a- Feldspar classification diagram. b- Clinopyroxene compositions plotted in the Ti vs. Ca+Na diagram (Leterrier *et al.*, 1982).

Fig. 6.- Composición mineral de los sill estudiados. a- Diagrama de clasificación de los feldespatos analizados. b- Composiones de clinopiroxeno representadas en el diagrama Ti vs. Ca+Na (Leterrier *et al.*, 1982).

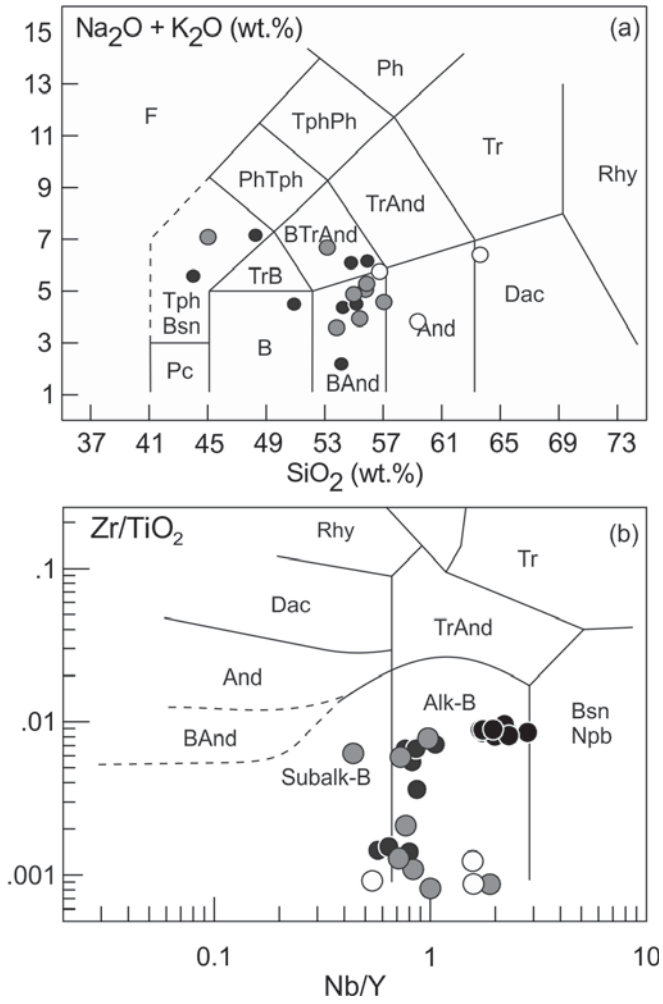

Fig. 7.- Total Alkalis vs. Silica (TAS) diagram (Le Bas *et al.*, 1986) (a) and Zr/TiO_2 vs. Nb/Y diagram (Winchester and Floyd, 1977) (b) applied to whole-rock compositions from the studied sills. Central facies: black circles; Chilled margin facies: grey circles; Pegmatoid facies: white circles.

Fig. 7.- Diagrama con Álcalis Total vs. Sílice (TAS) (Le Bas *et al.*, 1986) (a) y diagrama Zr/TiO_2 vs. Nb/Y (Winchester and Floyd, 1977) (b) aplicados a las composiciones de roca total de los sills estudiados. Facies central: círculos negros; Facies de borde enfriado: círculos grises; Facies pegmatoide: círculos blancos.

9 shows a slightly compatible behaviour of the transition elements (Cr, Ni) and a scattering of the large ion lithophile elements (LILE) and high field strength elements (HFSE). The light rare earth (LREE) and medium rare earth elements (MREE) show a general incompatible behaviour (Fig. 9), whereas the heavy rare earth elements (HREE), U and Th display a relative scattering, probably related to the presence of apatite in these rocks.

The high degree of alteration (Table 2) suggests that subsolidus processes may have played an important role in the final whole rock composition. The LILE and HFSE are highly mobilised during spilisation (e.g. Lago *et al*., 1989 and references therein; Shaw *et al*., 1977). Therefore, inmobile incompatible elements are preferred to define the geochemical affinity of these rocks. The Nb/Y ratios range between 0.44-1.89 (Table 2) indicating an alkaline affinity, in agreement with the orthose enrichment of the most albitic plagioclase (Fig. 6a). Moreover, Ti/V ratios range between 42 and 99 (Table 2), as typical for alkali basalts and oceanic island basalts (Shervais, 1982).

The chilled margin and central facies display the lowest REE abundances, whereas the pegmatoid facies presents the highest ones (Table 2). The primitive mantle-normalised incompatible ratios $(La/Yb)_N$ are similar in the chilled margin and central facies (2.32-14.55; Table 2) and are higher for the rocks of the pegmatoid facies (12.95-26.99; Table 2). The primitive mantle–normalised multielemental patterns are rather similar to each other (Fig. 10). The most incompatible elements are 10 to 200 times enriched over the primitive mantle. Most of the samples present strong Sr and Zr negative anomalies and enrichments in U and K. Furthermore, Rb, Ba, Ti and Eu display a relative variability. Finally, the LREE display subparallel patterns and the HREE show an increasing

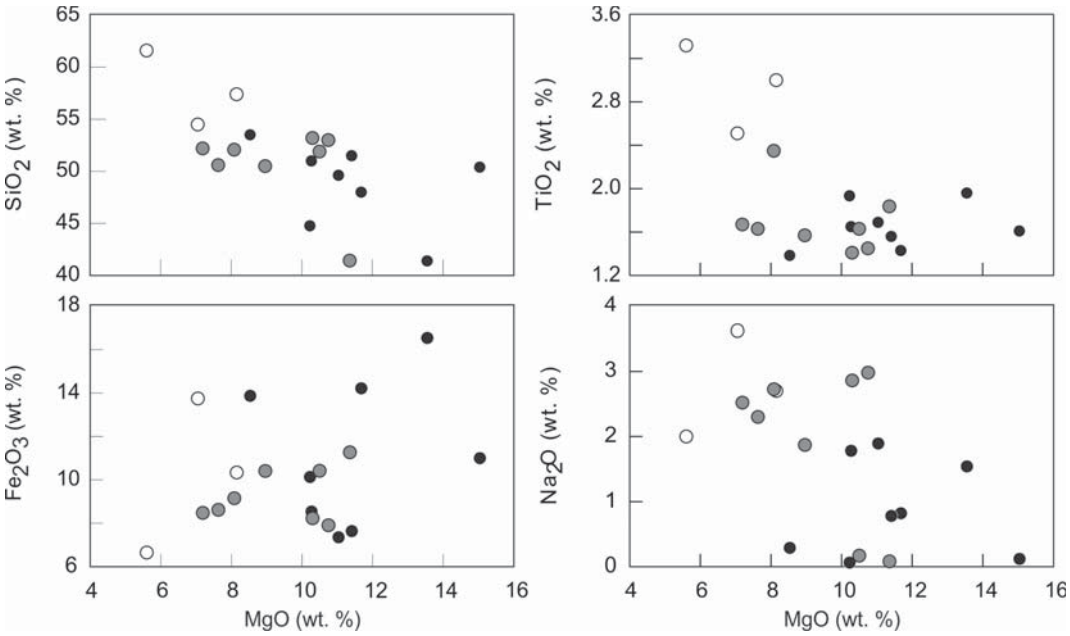

Fig. 8.- Whole-rock composition of the studied sills plotted in bivariate diagrams of major elements vs. MgO (wt. %). Symbols as in Fig. 7.

Fig. 8.- Composiciones de roca total de los sills estudiados representadas en diagramas bivariantes de elementos mayores frente a MgO (% en peso). Símbolos como en la Fig. 7.

slope from chilled margin and central facies to the pegmatoid facies.

7. Discussion

7.1. Emplacement and age of the magmatism

The igneous bodies are usually concordant to bedding planes, so they can be considered sill-like bodies. In the outcrops of the Moncayo sector only one igneous body (sill) is recognised. On the other hand, in the outcrops of the Cameros sector several igneous bodies are exposed. Sometimes, the igneous bodies are separated by thin sedimentary beds of argillites. In other cases, there is no separation in between and the sequence chilled margin – central facies is repeated several times. Therefore, they could belong to a single sill, sometimes filled by multiple pulses of magma. In each sector, the igneous outcrops cannot be clearly related to each other due to their considerable geographical dispersion. Accordingly, the occurrence of one or several sills per sector cannot be ascertained.

Bastida *et al*. (1989) described a low-grade contact metamorphism in the host-rocks of the Moncayo sector, related to the emplacement of the sills. The thickness of the sills in this sector ranges between 0.6 and 38 m. In the latter case, according to the heat transfer approximation by Jaeger (1968) and considering a thermal diffusivity of 10^{-6} m^2/s (Huppert and Sparks, 1980), the sill started cooling 42 days after the emplacement of the

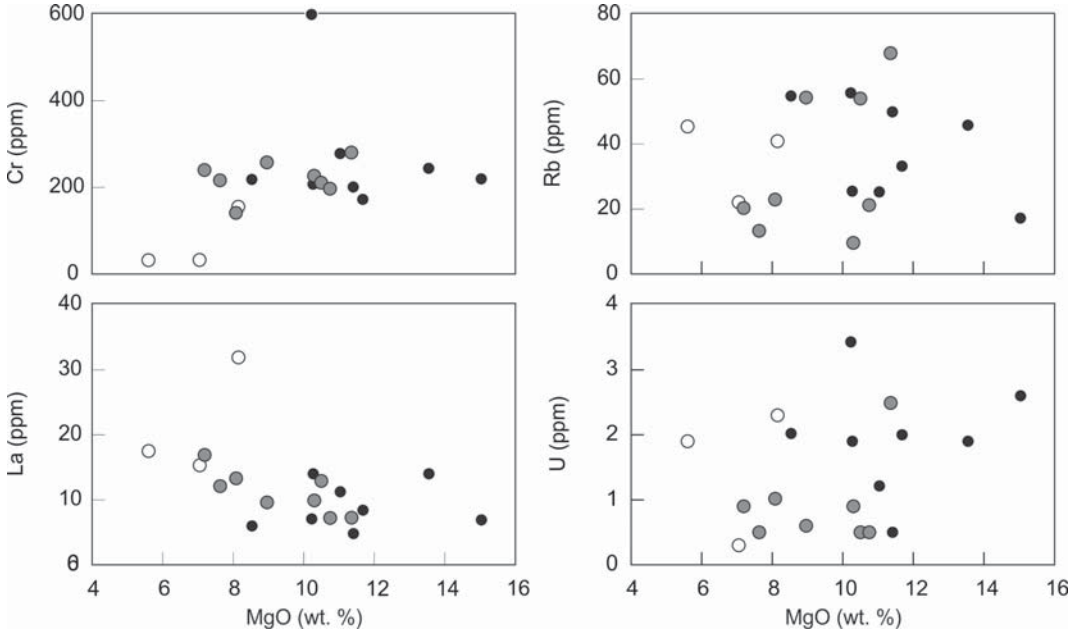

Fig. 9.- Whole-rock composition of the studied sills plotted in bivariate diagrams of trace elements vs. MgO (wt. %). Symbols as in Fig. 7.

Fig. 9.- Composiciones de roca total de los sills estudiados representadas en diagramas bivariantes de elementos traza frente a

magma and 418 days were needed to cool the centre of the sill. These results suggest a slow cooling rate, compatible with the development of the contact metamorphism in the sedimentary host-rock. The greater thickness of the sills in the Cameros sector (between 2 and 94 m) indicates even slower cooling rates; therefore, the development of contact metamorphism in this area cannot be ruled out.

The contacts of the sills are irregular and characterised by a peperitic transition zone (Fig. 4b). Peperites are typically developed where magma has come into contact with unconsolidated, wet sediments (Befus *et al*., 2009; Kano, 1991; Kano, 2002; Kokelaar, 1982; Lavine and Aalto, 2002; Leat and Thompson, 1988; Németh and Martin, 2007; Walker, 1992). The presence of sediment injections and irregular fragments of structure-less sediment at the lower contact of the sills (Fig. 4b and 4c) indicate that the unconsolidated host sediments were remobilised and injected through fractures into the sill and subsequently baked by contact metamorphism (Bastida *et al*., 1989; Busby-Spera and White, 1987; Gifkins *et al*., 2002; Kokelaar, 1982). The presence of vesicles trapped in the thickest igneous levels indicates that the magma emplaced into shallow and unconsolidated sediments.

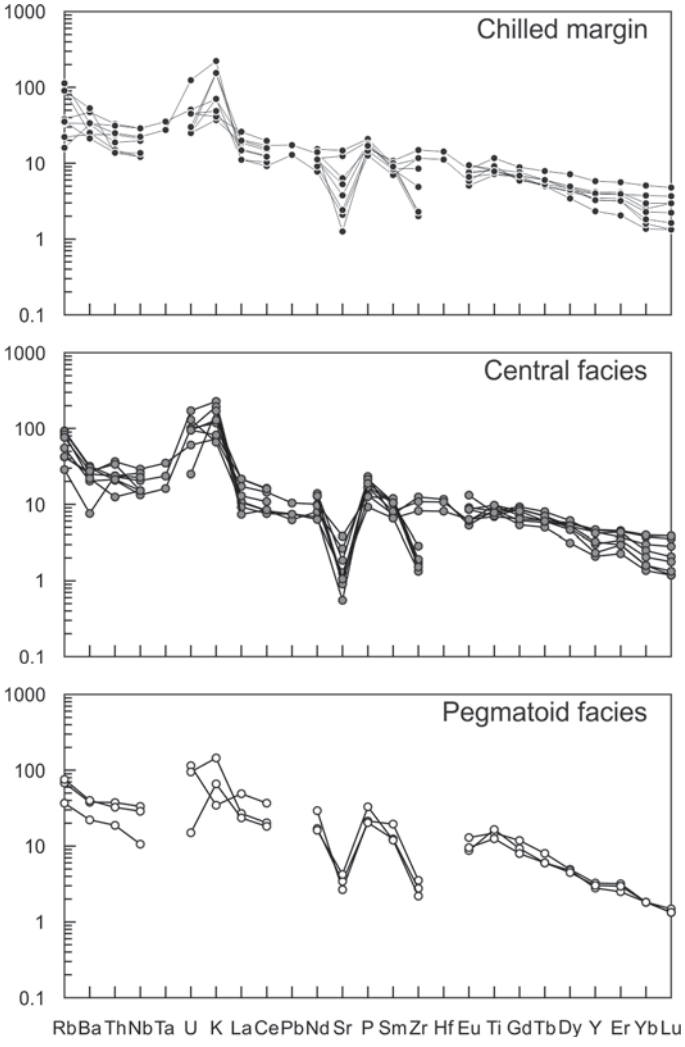

Fig. 10.- Primitive mantle-normalised multielemental diagrams of the studied sills. Normalising values are from McDonough and Sun (1995).

Fig. 10.- Diagramas multielementales de los sills estudiados, normalizado a manto primitivo. Los valores de normalización son de McDonough and Sun (1995).

The considerable alteration of the rocks (Table 2) prevents carrying out radiometric datings. However, the following field relationships are good indicators of the age of the igneous rocks: 1) first of all, the sills emplaced into the Keuper facies: 2), both the sills and the sedimentary host-rocks are affected by the Alpine deformation (e.g., Casas Sainz and Gil-Imaz, 1998; Guimerá *et al*., 2004), constraining the emplacement age of the sills to the Mesozoic; 3) in the Moncayo sector the conglomerates of the upper part of the Keuper facies include clasts of igneous rocks petrologically equivalent to the sills emplaced in the middle part of the Keuper facies (Lago *et al*., 1996), indicating an erosive and sedimentary phase between the emplacement of the sills and the sedimentation of the upper part of the Keuper facies; 4) the injections of sediment and the fragments of structure-less sediment from the host-rocks inside the sills, together with the development of peperites, as a whole indicate that the magma emplaced into wet, unconsolidated sediments. These arguments imply that the sills were emplaced during or shortly after the deposition of the Keuper facies sediments. Hence, the age of this magmatism can be defined as Upper Triassic.

Several differences between the emplacement styles of the igneous rocks in the two studied sectors can be highlighted. Firstly, the volume of exposed igneous rocks increases from the Moncayo sector (maximum thickness: 38 m) to the Cameros sector (maximum thickness: 94 m). Furthermore, in the outcrops of the Cameros sector multiple sills are recognised, in contrast with the single sills of the Moncayo sector. This difference suggests several pulses of magma in the Cameros sector and a single pulse in the Moncayo sector. Besides, the upper part of the Keuper facies is formed by a thin (up to 7 m thick) and homogeneous lacustrine sedimentary sequence in the Cameros sector, whereas it comprises an irregular alluvial-fluvial conglomeratic sequence related to an emerged continental area in the Moncayo sector. The spatial thickness variation of the conglomerate unit of the Moncayo sector and the size of its clasts suggest a proximal area located in the western part and the distal area located in the eastern part of this sector. The SW-NE main directions of the channel-shaped surfaces measured in the field suggest a possible source area close to the Tablado-Jarque fault. This is in agreement with the absence of the conglomeratic unit in the westermost outcrop of the Moncayo sector

(section 11; Fig. 3b), located at the hangingwall of this main Variscan fault.

Considering all the igneous outcrops, the volume of emplaced magma gradually increases from the SE to the NW (from Moncayo to Cameros). Furthermore, three areas of maximum thickness of exposed igneous rocks can be identified (Fig. 11): Cameros, Beratón and Arándiga (the latter two located in the Moncayo sector); these areas could be related to magma emission centres.

According to the exposed igneous thicknesses (Fig. 11), a close relationship between the distribution of the igneous rocks and the main fracture systems at a regional scale can be established (i.e. the Datos and the related Tablado-Jarque fault system; Fig. 2). Concerning the Cameros sector, the magma emplacement could be related to a master late-Variscan normal fault, corresponding to the present-day northern Cameros thrust (Casas Sainz and Gil-Imaz, 1998). On the other hand, the magma emplacement in the Moncayo area probably rose through a set of faults related to the master Datos fault (Fig. 2). Accordingly, it is suggested that the main magma emplacement in the NW sector of the Iberian Rift was probably linked to first-order late-Variscan normal faults.

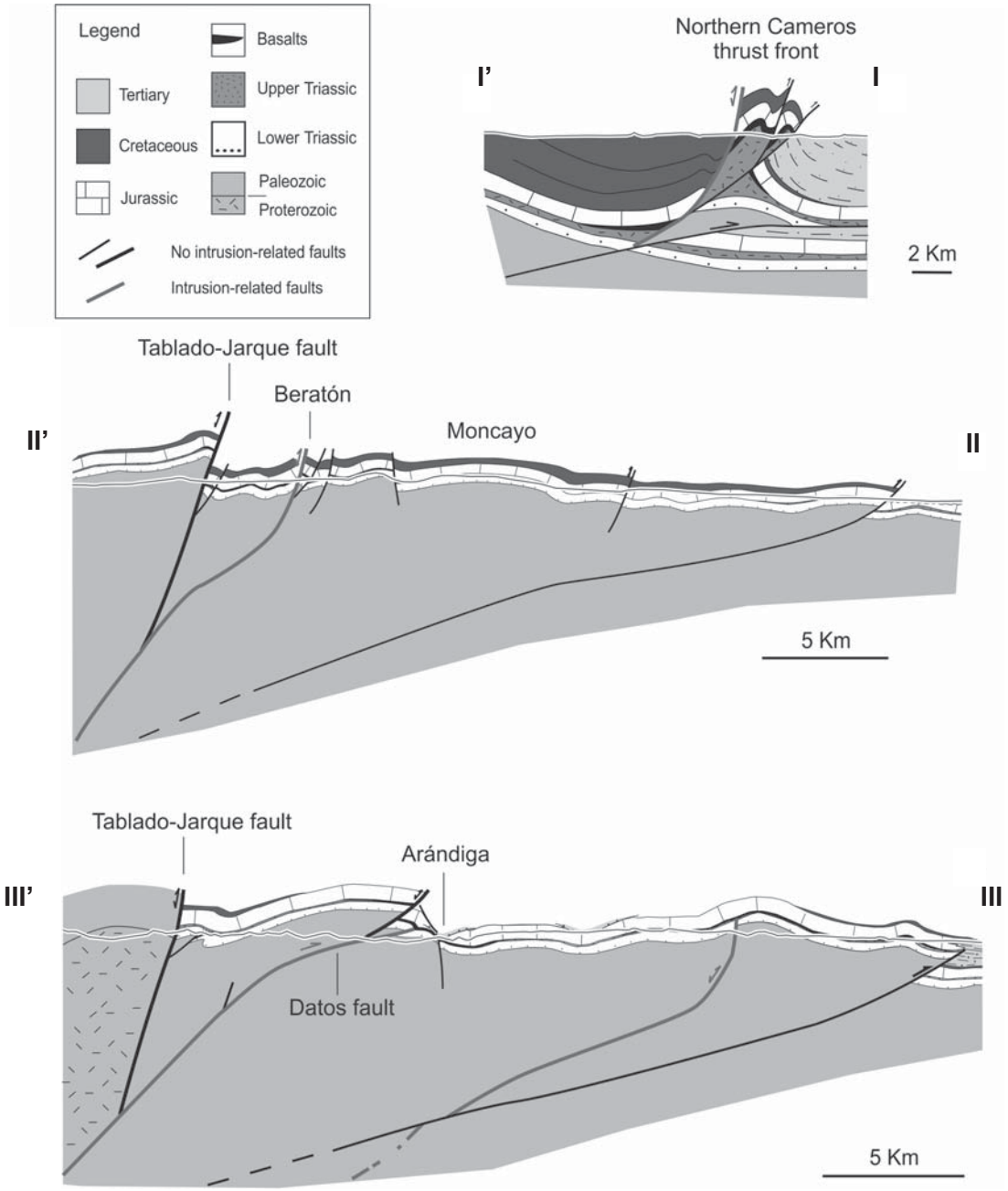

Fig. 11.- Cross sections in the studied sectors; location in Fig. 2.
Fig. 11.- Cortes geológicos de los sectores estudiados; localización en Fig. 2.

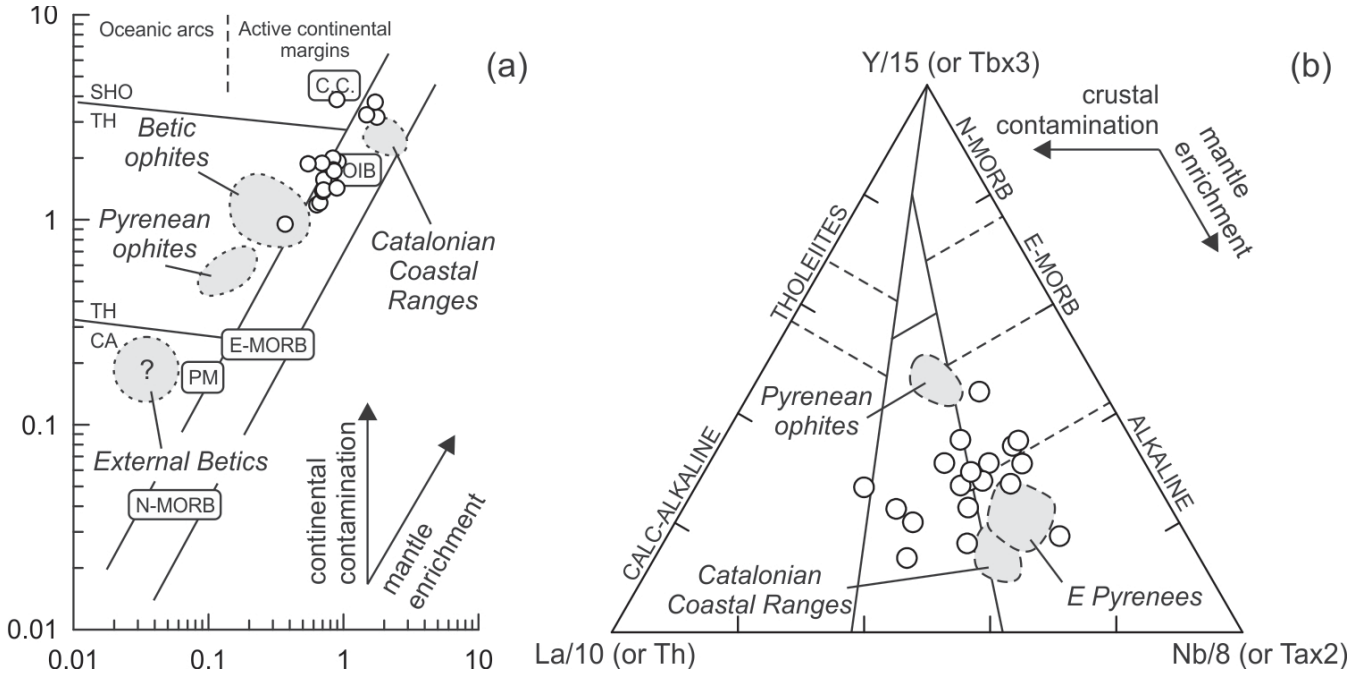

Fig. 12.- Comparison between the studied rocks and other Upper Triassic magmatisms in the eastern Iberian Peninsula. a- Th/Yb vs. Ta/Yb diagram (Pearce, 1983). b- La/10 – Y/15 – Nb/8 triangular diagram (Cabanis and Lecolle, 1989). SHO = shoshonitic series; CA = calc - alkaline series; TH = tholeiitic series. U.C. = average composition of the upper continental crust (after Taylor and McLennan, 1985). Primitive mantle (P.M.), N-MORB, E-MORB and OIB values from Sun and McDonough (1989). Comparison data from Beziat *et al*. (1991), Lago *et al*. (1996) and Morata *et al*. (1997). Ta contents, when absent, were calculated using a Nb/Ta = 16.

Fig. 12.- Comparación entre las rocas estudiadas y otros magmatismos del Triásico Superior de la parte oriental de la Península Ibérica. a- Diagrama Th/Yb vs. Ta/Yb (Pearce, 1983). b- Diagrama triangular La/10 – Y/15 – Nb/8 (Cabanis and Lecolle, 1989). SHO = serie shoshonítica; CA = serie calcoalcalina; TH = serie toleítica. U.C. = composición promedio de la corteza continental superior (despues de Taylor y McLennan, 1985). Los valores del Manto Primitivo (P.M.), N-MORB, E-MORB y OIB tomados de Sun y McDonough (1989). Datos para la comparación de Beziat *et al*. (1991), Lago *et al*. (1996) y Morata *et al*. (1997). Los contenidos de Ta, cuando están ausentes, han sido calculados según Nb/Ta = 16.

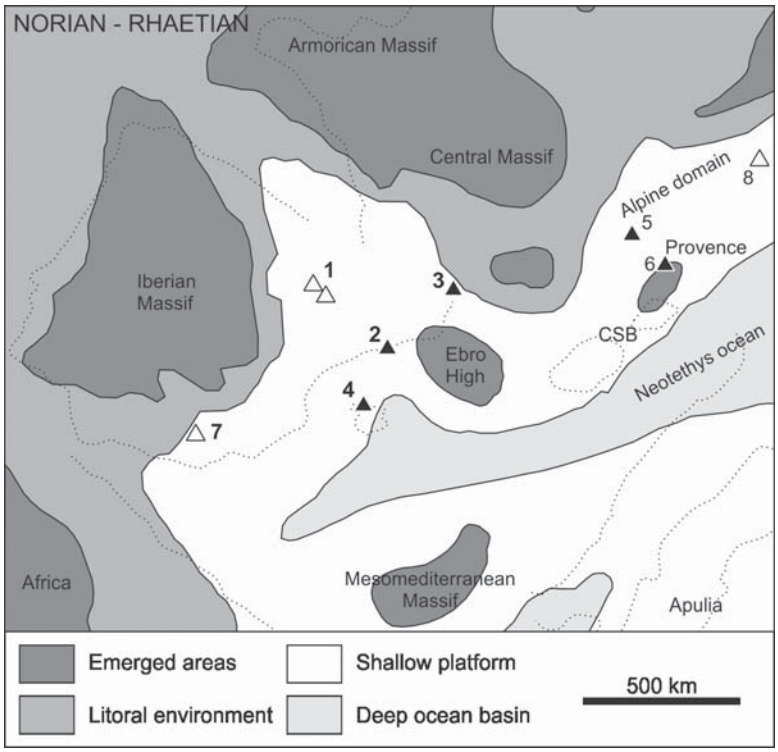

Fig. 13.- Paleogeographic scheme of the western part of the Neotethys realm during the the deposition of the Imón Fm and other equivalent units (Late Triassic) showing the location of the compared magmatisms. CSB: Corsica-Sardinia Block. Location of the magmatisms: 1) NW part of the Iberian Chain –this study-; 2) Catalonian Coastal Ranges (Tarragona); 3) Southern France; 4) Northern Range of Mallorca; 5) Écrins-Pelvoux Massif; 6) Provence; 7) External Betics; 8) Brescian Prealps. Modified from Pérez-López *et al*. (2012).

Fig. 13.- Esquema paleogeográfico de la parte occidental del Neotethys durante el depósito de la Fm. Imón y otras unidades equivalentes (Triásico Superior), mostrando la localización de los magmatismos comparados. CSB: Bloque de Córcega-Cerdeña. Localización de los magmatismos: 1) Parte NO de la Cadena Ibérica –este estudio-; 2) Cadenas Costero Catalanas (Tarragona); 3) Sur de Frnacia; 4) Sierra Norte de Mallorca; 5) Macizo de Écrins-Pelvoux; 6) Provenza; 7) Zona Externa de las Béticas; 8) Prealpes de Brescia. Modificado de Pérez-López *et al*. (2012).

7.2. Petrologic constraints and source of the magmatism

Based on field and petrographic relationships we have identified three facies in the studied sills: chilled margins, central facies and pegmatoids. All the facies have a similar mineralogy, although clinopyroxene has only been recognised in the central facies. However, the modal proportions vary from the chilled margin and central facies to the pegmatoid as follows: olivine decreases and plagioclase increases. Regarding the geochemical results, the chilled margins and the central facies show the most primitive compositions (lower SiO_2 and higher MgO contents; Table 2) whereas the pegmatoids present the most evolved compositions. Therefore, the distribution of the identified facies is related to a normal differentiation process from the margins of the sills inwards. The enrichments in SiO_2, TiO_2, Na_2O and incompatible trace elements (e.g., REE) in the pegmatoid are consistent with these rocks having crystallised from late-stage, more evolved melts. The differentiation process agrees with the slow cooling rate of the sills (more than 400 days) due to their large thickness.

The subsolidus processes (spilitisation) probably have substantially changed the original whole-rock composition, as revealed by the high value of LOI (Table 2) probably related to the replacement of original mineralogy by secondary minerals. This hypothesis is consistent with the presence of vesicles filled with quartz and chlorite. The subsolidus processes, together with the frequent host-rock xenoliths, could explain the anomalous enrichment in SiO_2 in these basic to intermediate rocks. Due to this extensive alteration and contamination, the mantle source of this magmatism is very hard to unravel. Nevertheless, some information can be drawn from the immobile trace elements.

The primitive mantle – normalised trace element patterns show a relative depletion in Nb and Ta (Fig. 10). This feature is characteristic of subduction-related melts or magmas affected by crustal contamination (Dupuy and Dostal, 1984; Dostal *et al*., 1986; Thompson *et al*., 1984). Nb/U ratios show an average value of 13 (Table 2) which is similar to the mean value of the continental crust and the island arc rocks (Nb/U ~ 10; Hofmann, 1997) and significantly lower than the value for OIB and MORB derived-rocks (Nb/U ~ 47; Hofmann, 1997). The K and U enrichments (Fig. 10) also support the crustal contamination of the magmas.

On the Th/Yb versus Ta/Yb diagram (Fig. 12a), the studied rocks plot within the mantle array between the OIB and the E-MORB compositions, suggesting the participation of an enriched subcontinental mantle source (Hawkesworth *et al*., 1983; Menzies *et al*., 1983; Morata *et al*., 1997, among others). Some of the samples have Th/Yb ratios more enriched than the OIB ratios suggesting crustal contamination. Similar conclusions can be drawn from the La/10, Y/15, Nb/8 triangular diagram (Fig. 12b) of Cabanis and Lecolle (1989), where the data plot between the alkaline and the E-MORB fields; in this diagram, the compositions are scattered and slightly enriched in the La/10 ratio, supporting crustal contamination.

7.3. Comparison with other Upper Triassic magmatisms of southwestern Europe: geodynamic implications

The Upper Triassic alkaline magmatic province of southwestern Europe was developed at the end of the Triassic rift stage and comprises outcrops in four sectors: NW part of the Iberian Range, south of the Catalonian Coastal Ranges, North Range of Mallorca and SE France (Corbieres, Écrins-Pelvoux and Provence; Azambre and Fabries, 1989; Lago *et al.*, 1996). This magmatic province was defined according to: 1) the similar mineralogical (olivine, Ti-rich augite, plagioclase and opaque minerals) and geochemical composition of the exposed rocks; 2) their alkaline affinity and 3) the presence of ultramafic xenoliths (Azambre and Fabries, 1989, Lago *et al.*, 1996). However, some differences between the outcrops of the NW part of the Iberian Chain and those of the other sectors of this province are identified. Firstly, the rocks of the NW part of the Iberian Chain have more evolved compositions (basalts to dacites), higher degrees of alteration (Table 2) and no peridotite xenoliths. Secondly, only subvolcanic rocks (sills) are recognised in the NW part of the Iberian Chain whereas subvolcanic rocks (sills and dikes) and phreatomagmatic rocks crop out in the other sectors of the province (Azambre and Rossy, 1981, Durand *et al*., 2011 and references therein, Mitjavila and Marti, 1985; Navidad and Álvaro, 1985; Sanz *et al*., 2012b, Vatin-Pérignon *et al*., 1974). Finally, the rocks exposed in the NW part of the Iberian Chain show geochemical evidences of the participation of an enriched subcontinental mantle source and a slight crustal contamination (Fig. 12a and b), whereas the rocks of the southern part of the Catalonian Coastal Ranges, the North Range of Mallorca and the Corbieres in SE of France suggest an asthenospheric mantle source with no significant crustal contamination (Fig. 12a and b).

Apart from the alkaline magmatic province proposed by Azambre and Fabries (1989) and Lago *et al*. (1996), other Upper Triassic magmatisms (late Carnian to Norian) related to the Triassic rift have been recognised in the external part of the Betic Cordillera (Pérez-López *et al*., 2012) and in the Brescian Prealps (Cassinis *et al*., 2008). The magmatism described in the Betic Cordillera emplaced into the Zamoranos Fm (Pérez-López *et al*.,

1992), which is correlated to the Imón Fm of the Iberian Chain (Pérez-López *et al*., 1992; López-Gómez *et al*., 1998; Arnal *et al*., 2002). The rocks are strongly altered and show field evidences of magma – sediment interaction, as the rocks of the northwestern Iberian Chain. According to Pérez-López *et al*. (2012), this magmatism is represented by sub-alkaline basalts to basaltic andesites deriving from a subcontinental upper mantle with assimilation of continental crust. A similar source has been inferred for the Late Carnian magmatism of the Brescian Prealps (Cassinis *et al*., 2008). These data suggest a likely similar mantle source and crustal contamination processes for the magmatisms of the NW part of the Iberian Chain, the external parts of the Betic Cordillera and the Brescian Prealps. However, no geochemical data are available for these sectors and a deep study would be necessary to prove this hypothesis.

The paleogeographic reconstruction of the western part of the Neotethys Realm during the Late Triassic shows an extensive epicontinental platform which correspond to the Imón Fm and other equivalent units (Fig. 13). The magmatism of this period is characterised by an asthenospheric source in the southeastern (inner) parts of the shallow platform (Catalonian Coastal Ranges and southern France) and by a progressively more sub-lithospheric mantle with a greater crustal contamination towards the western and northern (litoral) parts of this platform (NW Iberian Chain –this study-, External Betics and Brescian Prealps). These differences can be related to the thickness of the crust, which had to be thinner at the southeastern parts, allowing the melting of a deeper (asthenospheric) mantle. This is in agreement with the presence of ultramafic xenoliths only in the southeastern parts (Azambre and Fabries, 1989, Lago *et al.*, 1996; Sanz *et al*., 2012b). On the other hand, a thicker crust in the western and northern parts of the Neotethys realm conditioned the melting of a shallower sublithospheric mantle (E-MORB) and favoured the crustal contamination processes. A common geodynamic scenario for the Iberian Chain and the External Betics is consistent with the location of the Betic-Rif Cordillera and other terranes between the Iberian Peninsula and southern France until the Oligocene, as suggested by Rosenbaum *et al*. (2002 and references therein).

8. Conclusions

The Upper Triassic magmatism of the northwestern Iberian Chain is represented by sills of decametric thickness cropping out in two sectors: Cameros and Moncayo. This magmatism is characterised by a strong alteration (spilitisation) triggering mobilisation of LILE and HFSE. According to the interaction processes recognised between the magma and the host sediments, the emplacement of the magma took place during or shortly after the deposition of the Keuper facies. The presence of a conglomerate unit overlaying the sills in the Moncayo sector that contains clasts of similar igneous rocks strongly supports an Upper Triassic age for this magmatism.

The important thickness of the sills conditioned a slow cooling of the magma, triggering contact metamorphism of the host sediments and an internal differentiation of the magma bodies. From the sill margins inwards it shows: chilled margins, central facies and pegmatoid facies.

The source of this magmatism is inferred to be an enriched subcontinental mantle source involving an E-MORB component. The role of crustal contamination of the melts is clearly recognised. These source characteristics disagree with those recognised for other Upper Triassic magmatisms in northeastern Iberia and SE France. In contrast, similar rocks are found in the external Betic Cordillera and the Brescian Prealps. In the paleogeographical context of the Iberian plate in the Upper Triassic, the outcrops located in the inner platform area (Catalonian Coastal Ranges and SE France) present a deeper (asthenospheric) mantle source probably related to a thinner crust. On the contrary, the outcrops located in the outer platform (litoral) area (NW Iberian Chain –this study-, External Betics and Brescian Prealps) are characterised by a shallower, lithospheric mantle source involving crustal contamination.

Acknowledgements

We thank reviewers A. Ronchi and D. Gimeno and editors J. López-Gómez and J. Martín-Chivelet for their constructive comments which improved the original manuscript. The present work was financially supported by the 2010-edition of Research Grants of the IER (Instituto de Estudios Riojanos) of La Rioja Government, trough the project “Triassic magmatisms of the N Cameros Massif (La Rioja): environmental implications”.

References

Álvaro, M., Capote, R., Vegas, R. (1979): Un modelo de evolución geotectónica para la Cadena Celtibérica. *Acta Geológica Hispánica* 14, 172–177.

Arche, A., López-Gómez, J., (1996): Origin of the Permian–Triassic Iberian Basin, Central-Eastern Spain. *Tectonophysics* 266, 443–464. doi: 10.1016/S0040-1951(96)00202-8.

Arnal, I., Calvet, F., Márquez, L., Márquez-Aliaga, A., Solé de Porta, N. (2002): The epeiric carbonate plataform (Imón and Isábena Formations) of the Upper Triassic from the Northeastern Iberian Peninsula. *Acta Geologica Hispánica* 37 (4), 299–328.

Azambre, B., Fabriés, J. (1989): Mesozoic evolution of the upper mantle beneath the eastern Pyrenees; evidence from xenoliths in Tri-

assic and Cretaceous alkaline volcanoes of the eastern Corbières (France), *Tectonophysics* 170 (3–4), 213–230. doi: 10.1016/0040-1951(89)90272-2.

Azambre, B. and Rossy, M. (1981): Caractère alcalin du magmatisme triassique des Corbières orientales. *Bulletin de la Société Géologique de France* 23 (7), 253–262.

Bastida, J., Besteiro, J., Reventós, J.M., Lago, M., Pocovi, A. (1989): Los basaltos alcalinos subvolcánicos espilitizados de Arándiga (provincia de Zaragoza): estudio mineralógico y geoquímico. *Acta Geológica Hispánica* 24 (2), 115–130.

Befus, K.S., Hanson, R.E., Miggins, D.P., Breyer, J.A., Busbey, A.B. (2009): Nonexplosive and explosive magma/wet-sediment interaction during emplacement of Eocene intrusions into Cretaceous to Eocene strata, Trans-Pecos igneous province, West Texas. *Journal of Volcanology and Geothermal Research* 181 (3–4), 155–172. doi: 10.1016/j.jvolgeores.2008.12.017.

Beziat, D., Joron, J.L., Monchoux, P., Treuil, M., Walgenwitz, F. (1991): Geodynamic implications of geochemical data for the Pyrenean ophites (Spain-France). *Chemical Geology* 89, 243–262. doi: 10.1016/0009-2541(91)90019-N.

Busby-Spera, C.J., White, J.D.L. (1987): Variation in peperite textures associated with differing host-sediment properties. *Bulletin of Volcanology* 49, 765–775. doi: 10.1007/BF01079827.

Cabanis, B., Lecolle, M. (1989): Le diagramme La/10 - Y/15 - Nb/8: un outfil pour la discrimination de series volcaniques et la mise en evidence des processus de mélange et/ou de contamination crustale. *Comptes Rendus de l'Academie des Sciences (Sèrie II)* 309, 2023–2029.

Cabral, A.R., Beaudoin, G. (2007): Volcanic red-bed copper mineralisation related to submarine basalt alteration, Mont Alexandre, Quebec Appalachians, Canada. *Mineralium Deposita* 42 (8), 901–912. doi: 10.1007/s00126-007-0141-7.

Casas-Sainz, A.M., Gil-Imaz. A. (1998): Extensional subsidence, contractional folding and thrust inversion of the eastern Cameros basin, northern Spain. *Geologische Rundschau* 86 (4), 802–818. doi: 10.1007/s005310050178.

Cassinis, G., Cortesogno, L., Gaggero, L., Perotti C.R. and Buzzi, L. (2008): Permian to Triassic geodynamic and magmatic evolution of the Brescian Prealps (eastern Lombardy, Italy). *Italian Journal of Geosciences* 127 (3), 501–518.

Dostal., J., Baragar, R.A., Dupuy, C. (1986): Petrogenesis of the Natkusiak continental basalts, Victoria Island, Northwest Territories, Canada. *Canadian Journal of Earth Sciences* 23 (5), 622–632. doi: 10.1139/e86-064.

Droop, G.T.R. (1987): A general equation for estimating Fe^{3+} concentrations in ferromagnesian silicates and oxides from microprobe. *Mineralogical Magazine* 57, 431–435. doi: 10.1180/minmag.1987.051.361.10.

Dupuy, C., Dostal., J. (1984): Trace element geochemistry of some continental tholeiites. *Earth and Planetary Science Letters* 67 (1), 61–69. doi: 10.1016/0012-821X(84)90038-4.

Durand, M., Caron, J.P., Hagdorn, H. (2011): *Pan-European Correlation of the Triassic 8th International Field Workshop. Triassic of Southeast France (Provence: Var & Alpes-Maritimes)*. Association des Géologues du Permien et du Trias, 66 p.

Frey, F.A., Green, D.H., Roy, S.D. (1978): Integrated models of basalt petrogenesis - study of quartz tholeiites to olivine melilities from South Eastern Australia utilizing geochemical and experimental petrological data. *Journal of Petrology* 19 (3) 463–513. doi: 10.1093/petrology/19.3.463.

Gibbs, A.D. (1984): Structural evolution of extensional basin margins. *Journal of the Geological Society London* 141, 609–620. doi: 10.1144/gsjgs.141.4.0609.

Gifkins, C.C., McPhie, J., Allen, R.L. (2002): Pumiceous rhyolitic peperite in ancient submarine volcanic successions. *Journal of Volcanology and Geothermal Research* 114, 181–203. doi: 10.1016/S0377-0273(01)00284-0.

Goy, A., Yébenes, A. (1977): Caracterización, extensión y edad de la Formación Dolomías Tableadas de Imón. *Cuadernos de Geología Ibérica* 4, 375–384.

Guimera, J., Mas, R., Alonso, A. (2004): Intraplate deformation in the NW Iberian Chain: Mesozoic extension and Tertiaty contractional inversion. *Journal of the Geological Society London* 161, 291–303. doi: 10.1144/0016-764903-055.

Hawkesworth, C., Erlank, A., Marsh, J., Menzies, M., Van Calsteren, P. (1983). Evolution of the continental lithosphere: evidence from volcanics and xenoliths in southern africa. In: Hawkesworth, C. J. & Norry, M. J. (eds.) *Continental Basalts and Mantle Xenoliths*. Shiva Press, Orpington, 111−138.

Hofmann, A.W. (1997): Mantle geochemistry: the message from oceanic volcanism. *Nature* 385, 219–229. doi: 10.1038/385219a0.

Huppert, H.E., Sparks, R.S.J. (1980): Restrictions on the compositions of mid-ocean ridge basalts: a fluid dynamical investigation. *Nature* 286, 46–48. doi: 10.1038/286046a0.

Jaeger, J.C. (1968): Cooling and solidification of igneous rocks. In: Hess, H.H., Poldervaart, A. (eds.), *Basalts: The Poldervaart Treatise on Rocks of Basaltic Compositions*. Wiley Interscience, New York, 503–536.

Kano, K. (1991): Miocene pillowed sills in the Shimane Peninsula, SW Japan. *Journal of Volcanology and Geothermal Research* 48, 359–366. doi: 10.1016/0377-0273(91)90051-Z.

Kano, K. (2002): Middle Miocene volcaniclastic dikes at Kukedo, Shimane Peninsula, SW Japan: fluidization of volcaniclastic beds by emplacement of syn-volcanic andesitic dikes. *Journal of Volcanology and Geothermal Research* 114, 81–94. doi: 10.1016/S0377-0273(01)00283-9.

Kokelaar, B.P. (1982): Fluidization of wet sediments during the emplacement and cooling of various igneous bodies. *Journal of the Geological Society* 139, 21–33. doi: 10.1144/gsjgs.139.1.0021.

Lago, M., Vaquer, R., Zachmann, D., Pocovi, A., Torres, J.A., Enrique, P. (1989): Estudio Geoquímico de procesos de espilitización afectando a basaltos alcalinos, Keuper terminal-Rhetiense, en la Cadena Ibérica, Cadenas Costeras Catalanas y Sierra Norte de Mallorca, *Actas del I Congreso Ibérico de Geoquímica* I, 139–150.

Lago, M., Pocovi, A., Bastida, J., Arranz, E., Vaquer, R., Dumitrescu, R., Gil-Imaz, A., Lapuente, M.P. (1996): El magmatismo alcalino, hettangiense, en el dominio nor-oriental de la Placa Ibérica. *Cuadernos de Geología Ibérica* 20, 109–138.

Lavine, A., Aalto, K.R. (2002): Morphology of a crater-filling lava lake margin, The Peninsula tuff cone, Tule Lake National Wildlife Refuge, California: implications for formation of peperite textures. *Journal of Volcanology and Geothermal Research* 114, 147–163. doi: 10.1016/S0377-0273(01)00285-2.

Leat, P.T., Thompson. R.N. (1988): Miocene hydrovolcanism in NW Colorado, USA, fueled by explosive mixing of basic magma and wet unconsolidated sediment. *Bulletin of Volcanology* 50, 229–243. doi: 10.1007/BF01047486.

Le Bas, M.J., Le Maitre, R.W., Streckeisen, A., Zanettin, B. (1986): A chemical classification of volcanic rocks based on the total alkali-silica diagram. *Journal of Petrology* 27, 745–750. doi: 10.1093/petrology/27.3.745.

Leterrier, J., Mauri, R.C., Thonon, P., Girard, D., Marchal, M. (1982): Clinopyroxene composition as a method identification of the magmatic affinities of paleo-volcanic series. *Earth and Planetary Science Letters* 59, 139–154. doi: 10.1016/0012-821X(82)90122-4.

López Gómez, J., Más, R., Arche, A. (1993): The evolution of the Middle Triassic (Muschelkalk) carbonate ramp in the SE Iberian Ranges, eastern Spain: sequence stratigraphy, dolomitisation pro-

cesses and dynamic controls. *Sedimentary Geology* 87, 165–193. doi: 10.1016/0037-0738(93)90003-N.

López-Gómez, J., Arche, A., Calvet, F., Goy, A. (1998): Epicontinental marine carbonate sediments of the Middle and Upper Triassic in the westernmost part of the Tethys Sea, Iberian Peninsula. In: Bachmann, G.H., Lerche, I. (Eds.), *Epicontinental Triassic*: Zentralblatt für Geologie und Paläontologie I, 1033–1084.

López Gómez, J., Arche, A., Pérez López, A. (2002): Permian and Triassic. In: Gibbons, W., Moreno, M.T. (Eds.) *The Geology of Spain*. Geological Society, London, 185–212.

McDonough, W.F., Sun, C.C. (1995): Composition of the Earth. *Chemical Geology* 120, 223–253. doi: 10.1016/0009-2541(94)00140-4.

Menzies, M.A., Leeman, W.P., Hawkesworth, C.J. (1983): Isotope geochemistry of Cenozoic volcanic rocks reveals mantle heterogeneity below western USA. *Nature* 303, 205–209. doi: 10.1038/303205a0.

Mitjavila, J., Marti, J. (1986): El volcanismo triásico del sur de Catalunya. *Revista del Instituto de Investigaciones Geológicas* 42/43, 89–103.

Morata, D., Puga, E., Demant, A., Aguirre, L. (1997): Geochemistry and tectonic setting of the «ophites» from the external zones of the Betic Cordilleras (s. Spain). *Estudios Geológicos* 53, 107–120. doi: 10.3989/egeol.97533-4236.

Morimoto, N., Fabries, J., Ferguson, A. K., Ginzburg, I. V., Ross, M., Seifert, F. A., Zussman, J., Aoki, K., Gottardi, G. (1988): Nomenclature of pyroxenes. *American Mineralogist* 73, 1123–1133. doi: 0003-004X/88/0910-1123$02.00.

Morley, C.K. (1999): Boundary fault angle with particular reference to the Lokichar fault, Turkana region, Kenya. In: Morley, C.K. (Ed.) *Geoscience of Rift Systems-Evolution of East Africa*. AAPG 44, 115–130.

Navidad, M., Álvaro, M. (1985): El vulcanismo alcalino del Triásico Superior de Mallorca (Mediterráneo Occidental). *Boletín Geológico y Minero* 96 (1), 10–22.

Németh, K., Martin, U. (2007): Shallow sill and dyke complex in western Hungary as a possible feeding system of phreatomagmatic volcanoes in "soft-rock" environment. *Journal of Volcanology and Geothermal Research* 159, 138–152. doi: 10.1016/j.jvolgeores.2006.06.014.

Pearce, J. A (1983). Role of sub-continental lithosphere in magma genesis in active continental margins. In: Hawkesworth, C. J., and Norry, M. J., (eds.) *Continental basalts and mantle xenoliths,* Shiva Geology Series. Birkhouser Boston, 230–249.

Pérez-López, A., Pérez-Valera, F. (2007): Palaeogeography, facies and nomenclature of the Triassic units in the different domains of the Betic Cordillera (S Spain). *Palaeogeography, Paleoclimatology, Palaeoecology* 254, 606–626. doi: 10.1016/j.palaeo.2007.07.012.

Pérez-López, A., Pérez-Valera, F., Götz, A. (2012): Record of epicontinental platform evolution and volcanic activity during a major rifting phase: The Late Triassic Zamoranos Formation (Betic Cordillera, S Spain). *Sedimentary Geology* 247/248, 39–57. doi: 10.1016/j.sedgeo.2011.12.012.

Pérez-López, A., Solé de Porta, N., Márquez, L., Márquez-Aliaga, A. (1992): Caracterización y datación de una unidad carbonática de edad Noriense (Fm. Zamoranos) en el Trías de la Zona Subbética. *Revista de la Sociedad Geológica de España* 5, 113–127.

Rosenbaum, G., Lister, G.S., Duboz, C. (2002): Reconstruction of the tectonic evolution of the western Mediterranean since the Oligocene. In: Rosenbaum, G. and Lister, G.S. (Eds.) *Reconstruction of the evolution of the Alpine-Himalayan Orogen*. Journal of the Virtual Explorer 8, 107–126. doi: 10.3809/jvirtex.2002.00053.

Salas, R., Casas, A. (1993): Mesozoic extensional tectonics, stratigraphy and crustal evolution during the Alpine cycle of the eastern Iberian basin. *Tectonophysics* 228, 33–55. doi: 10.1016/0040-1951(93)90213-4.

Sanz, T., Lago, M., Gil, A., Pocovi, A., Galé, C., Ubide, T., Ramajo, J., Tierz, P. (2012a): Magmatismo alcalino del Triásico Superior (Noriense) en el extremo NO de la Rama aragonesa de la Cordillera Ibérica: Modelo de emplazamiento en relación a fallas sin-sedimentarias. *Geogaceta* 51, 3–6.

Sanz, T.; Lago, M.; Gil, A.; Galé, C.; Ubide, T.; Larrea, P.; Ramajo, J.; Tierz, P. y Pocoví, A. (2012b). Estratigrafía y petrología de la región volcánica del Baix Ebre (Tarragona): etapas y edad del magmatismo. *Geogaceta* 52: 33-36.

Shaw, D.M., Vatin-Pérignon, N., Muysson, J.R. (1977): Lithium in spilites. *Geochimica et Cosmochimica Acta* 41 (11), 1601–1607. doi: 10.1016/0016-7037(77)90171-5.

Shervais, J.W. (1982): Ti–V plots and the petrogenesis of modern and ophiolitic lavas. *Earth and Planetary Sciences Letters* 59, 101–118. doi: 10.1016/0012-821X(82)90120-0.

Skilling, I.P., White, J.D.L., McPhie, J. (2002). Peperite: a review of magma–sediment mingling. *Journal of Volcanology and Geothermal Research* 114, 1–17. doi: 10.1016/S0377-0273(01)00278-5.

Sopeña, A., López Gómez, J., Arche, A., Pérez Arlucea, M., Ramos, A., Virgili, C., Hernando, S. (1988): Permian and Triassic rift basins of the Iberian peninsula. In: Manspeizer, W. (Ed.) *Triassic-Jurassic Rifting. Continental Break-up and Origin of the Atlantic Ocean and Passive Margins*. Developments in Geotectonics, 22B. Elsevier, Amsterdam, 757–786.

Sun, S.S., McDonough, W.F. (1989): Chemical and isotopic systematics of oceanic basalts: implications for mantle composition and processes. In: Saunders, A.D. and Norry, M.J. (eds.) *Magmatism in the Ocean Basins*. Special Publications 42, The Geological Society, London, 313–345.

Taylor, S.R., McLennan, S.M. (1985): *The continental crust: its composition and evolution*. Blackwell, Oxford, 312 p.

Thompson, R.N., Hendry, G.L., Parry, S.J. (1984): An assessment of the relative roles of crust and mantle in magma genesis: and elemental approach. *Philosophical Transactions of the Royal Society of London* 310, 549–590. doi: 10.1098/rsta.1984.0008.

Vatin-Pérignon, N., Aumaitre, R., Buffet, G. (1974): La spilitisation dans le massif des Écrins-Pelvoux: un cortège intrusif et effusif dolérito-spilitique (Alpes françaises occidentales). *Géologie Alpine*, 50, 153–194.

Vargas, H., Gaspar Escribano, J.M., López Gómez, J., VanWees, J.D., Cloetingh, S., De La Horra, R., Arche, A. (2009): A comparison of the Iberian and Ebro Basins during the Permian and Triassic, eastern Spain: A quantitative subsidence modeling approach. *Tectonophysics* 474: 160–183. doi: 10.1016/j.tecto.2008.06.005.

Walker, G.P.L. (1992): Morphometric study of pillow-size spectrum among pillow lavas. *Bulletin of Volcanology* 54, 459–474. doi: 10.1007/BF00301392.

Wernicke, B., Tilke, P. (1989): Extensional tectonic framework of the U.S. Central Atlantic Passive Margin. In: Tankard, A., Balkwill, H.R. (Eds.), *Extensional tectonics and stratigraphy of the northern Atlantic margins*. AAPG 46, 7–21.

White, J.D.L., McPhie, J., Skilling, I., (2000): Peperite: a useful genetic term. *Bulletin of Volcanology* 62, 65–66. doi: 10.1007/s004450050293.

Whitney, D.L., Evans, B.W. (2010): Abbreviations for names of rock-forming minerals. *American Mineralogist* 95 (1), 185–187. doi: 10.2138/am.2010.3371.

Winchester, J.A., Floyd, P.A. (1977): Geochemical discrimination of different magma series and their differentiation products using immobile elements. *Chemical Geology* 20, 325–343. doi: 10.1016/0009-2541(77)90057-2.